study, we focused on early growth response 4 (*EGR4*), which is significantly upregulated in bone metastatic tumors compared with other organ metastases (lung, kidney and liver) derived from human SCLC cells [7].

The *EGR4* gene belongs to the early growth response family of immediate early genes encoding four DNA-binding, zinc-finger transcription factors (*EGR1* to *EGR4*) [8]. This gene (*pAT133*, *NGFI-C*) was first identified as a zinc-finger protein immediately induced by mitogenic stimulation in T lymphocytes and fibroblasts [9,10]. It has been reported that *EGR4*-null mice have male infertility because of arrested spermatogenesis but no female infertility is observed [11,12], suggesting that EGR4 plays a critical role in some types of human idiopathic male infertility. Moreover, EGR4 is known to have a neural-specific expression pattern in rats [13] and regulate brain-derived neurotrophic factor (BDNF)-mediated neuron-specific potassium chloride cotransporter 2 (KCC2) transcription via the ERK1/2 signaling pathway in immature neurons [14]. However, the pathophysiological role of EGR4 in carcinogenesis in SCLC, has not been elucidated. In this study, we report that EGR4 acts as a transcriptional activator via regulation of specific downstream genes in SCLC cell proliferation.

Materials and Methods

Cell lines

The human SCLC cell lines SBC-3 and SBC-5 were kindly provided by Drs. M. Tanimoto and K. Kiura of Okayama University [15]. The NSCLC cell line PC14PE6 was kindly provided by Dr. I. J. Fidler of M. D. Anderson Cancer Center [16]. The human SCLC cell line NCI-H1048 and human NSCLC cell lines A549 and NCI-H1048 were purchased from the American Type Culture Collection (ATCC, Rockville, MD, USA). The human ACC-LC319/bone2 cell line was established as previously described [17]. The MC3T3-E1 murine osteoblastic subclone 4 cell line was kindly provided by Chugai Pharmaceutical Co., Ltd. (Tokyo, Japan). The human small airway epithelial cell line (SAEC) was purchased from Lonza (Walkersville, MD, USA). All cells were cultured under appropriate conditions.

Plasmid constructs

The entire coding sequence of human *EGR4* (NM_001965) was amplified by PCR using KOD plus DNA polymerase (Toyobo, Osaka, Japan). The PCR product was inserted into the *Eco*RI and *Xho*I sites of the pCAGGSn3FH vector which contains an N-terminal FLAG tag. For luciferase reporter plasmids, DNA fragments from the 5′-flanking regions of *PTHrP-V3* and *V4* (NM_198964.1 and NM_198966.1, respectively), *SAMD5* (NM_001030060.2), *RAB15* (NM_198686.2), *SYNPO* (NM_007286.5) and *DLX5* (NM_005221.5), which include potential EGR binding sites as predicted by the MatInspector program (Genomatix, http://www.genomatix.de/matinspector.html), were amplified by PCR and inserted into the appropriate restriction enzyme sites in the pGL3-enhancer vector (Promega, Madison, WI, USA). The PCR primer sets used in this study are shown in Table S1. The DNA sequences of all constructs were confirmed by DNA sequencing (ABI 3500xL sequencer; Life Technologies, Foster City, CA, USA).

RNA extraction, reverse transcription, semi-quantitative PCR and real-time PCR

Total RNA extraction, reverse-transcription, semi-quantitative RT-PCR and Real-time PCR experiments were conducted as previously described [18]. The expression levels in each sample were normalized to the β-actin mRNA content. The sequences of each primer set are listed in Table S2.

Western blot analysis

Western blot analysis was performed as previously described [18]. After SDS-PAGE, membranes blotted with proteins were incubated with anti-FLAG M2 (Sigma-Aldrich, St. Louis, MO, USA, F3165) or anti-β-actin (AC-15, Sigma-Aldrich, A-5441) mouse monoclonal antibodies diluted at 1:5000. The membranes were then incubated with a horseradish peroxidase (HRP)-conjugated secondary antibody for 1 h, and the protein bands were visualized with enhanced chemiluminescence (ECL) detection reagents (GE Healthcare, Piscataway, NJ, USA).

Measurement of PTHrP secretion

HEK293T cells (1.5×10^5 cells/12-well plate) were transfected with the pCAGGSn3FH-EGR4 or mock (no insert) plasmids using FuGENE 6 (Promega). At 48 h after transfection, the culture medium was collected and centrifuged at 4°C at 15,000 rpm. The PTHrP protein concentration in the conditioned media was determined by an immunoradiometric (IRMA) assay (SRL Inc., Tokyo, Japan).

Effect of conditioned medium derived from EGR4-overexpressing HEK293T cells on *RANLK*, *IL-6* and *IL-8* expression

HEK293T cells (2.6×10^6 cells/10 cm plate) were transiently transfected with the pCAGGSn3FH-EGR4 or mock vector for 48 h, and the culture media was then replaced with DMEM plus 0.1% FBS for an additional 48 h. The culture medium was subsequently collected, and the conditioned medium was transferred to murine MC3T3-E1 osteoblast cells that were pre-cultured with differentiation medium containing ascorbic acid (100 μg/ml) for 5 days. After 48 h, the expression levels of murine *RANKL*, *IL-6*, and *IL-8* was analyzed by real-time PCR as described above.

Chromatin immunoprecipitation (ChIP) assay

HEK293T cells (2.5×10^6 cells/10 cm dish) were transfected with 8 μg of the pCAGGSn3FH-EGR4 or mock vector for 48 h and then ChIP assays were performed using the EZ-ChIP kit (Millipore, Billerica, MA, USA) as previously described [19]. The PCR primer sets to detect the EGR-binding sites used are listed in Table S3.

Luciferase assay

HEK293T cells (2.5×10^4 cells/48-well dish) were co-transfected with either 100 ng of the pGL3-enhancer promoter vector as described above or the mock vector in combination with 100 ng of the pCAGGSn3FH-EGR4 or mock vector (100 ng). pRL-TK was used as an internal control. After 48 h, the cells were harvested and analyzed for *Firefly* luciferase and *Renilla* luciferase activity using the dual luciferase reporter assay (Promega) as previously described [19]. Data were expressed as the fold increase over mock-transfected cells (set at 1.0) and represented as the mean ± SE of two independent experiments.

NIH3T3 cell proliferation assay

NIH3T3 cells (0.5×10^5 cells/6-well dish) were transiently transfected with 3 μg of pCAGGSn3FH-EGR4 or mock vector using FuGENE 6 (Promega). Cell proliferation assays were performed at 48, 72 and 96 h after transfection, respectively, using Cell Counting Kit-8 (Dojindo, Kumamoto, Japan) as

previously described [18]. These experiments were performed in triplicate. Western blot analysis was performed as described above.

Gene silencing effects by siRNA treatment

We used siRNA oligonucleotides (Sigma-Aldrich Japan KK, Japan) to knock down *EGR4*, *DLX5*, *SYNPO SAMD5* and *RAB15* expression in SBC-5, SBC-3, NCI-H1048 or PC14PE6. The sequences targeting each gene are listed in Table S4. Cells were plated in 12-well dishes (SBC-5 and PC14PE6; 1.5×10^4 cells/well, SBC-3; 2.5×10^4 cells/well, NCI-H1048; 5.0×10^4 cells/well). Transfection of 100 nM siRNA to SBC-5 and PC14PE6 cells was performed using Lipofectamine 2000 reagent (Life Technologies) as previously described [20]. SBC-3 and NCI-H1048 cells were transfected with 50 nM siRNAs using Lipofectamine RNAi Max transfection reagent (Life Technologies) according to the manufacturer's instructions. At 48, 96 or 120 h after transfection, total RNA extraction, real-time PCR and cell proliferation assays were performed as described above.

Identification of EGR4 downstream genes by DNA microarray

SBC-5 cells (1×10^6 cells/35 mm dish for 24 h) were transfected with 10 nM siRNA directed against EGR4 (EGR4-2) or EGFP (siEGFP; a control) using Lipofectamine RNAi Max transfection reagent (Life Technologies). Total RNA was extracted from each sample at 48 and 72 h after transfection of siRNA. The DNA microarray and data analyses were performed using the Agilent Whole Human Genome Microarray (4×44K, G4110F; Agilent Technologies, Santa Clara, CA, USA) and GeneSpring software (version 11.5; Agilent Technologies) as previously described [21]. A corrected *P* value was calculated with Benjamini Hochberg false discovery rate (FDR) analysis, and $P<0.05$ was considered significant. The extent and direction of the differential expression between time points (48 and 72 h) were determined by calculating fold change values. The DNA microarray analysis data have been submitted to the NCBI Gene Expression Omnibus (GEO) database as series GSE40558.

RNAseq data analysis of lung cancers

Publicly available gene expression data (normalized values from Illumina RNAseq v2, level 3, LUAD and LUSC) from The Cancer Genome Atlas (TCGA; http://cancergenome.nih.gov/) were downloaded from TCGA matrix. The differential expression (by fold change value) between cancer tissues and the adjacent normal lung was calculated according to the normalized gene expression value of each sample.

Statistical analysis

Statistical analysis was performed using Student's *t*-test. $P<0.05$ was considered significant.

Results

EGR4 directly regulates the transcriptional activity of the *PTHrP* gene

Analysis of the genome-wide gene expression profile of the organ-preferential metastasis of the human SCLC cell line SBC-5 in mice identified early growth response 4 (*EGR4*), which was significantly upregulated in bone metastatic tumors ($p<0.001$, ratio; 2.22) compared with other organ metastases (lung, kidney and liver) [7]. First, to clarify the role of EGR4 as a transcription factor involved in bone metastasis, we focused on the parathyroid hormone-related protein (*PTHrP*) gene as a candidate downstream target of EGR4 because the *PTHrP* gene is known to be a potent activator of osteoclastic bone resorption [4] and encodes a protein secreted from SBC-5 cells [22,23]. Moreover, it has been reported that treatment with an anti-PTHrP neutralizing antibody inhibits the production of SBC5 cell bone metastasis in the SCID mouse model [22,23].

In the National Center for Biotechnology Information (NCBI) database, the *PTHrP* gene is reported to possess four transcriptional variants, designated *PTHrP* variant 1 (PTHrP-V1, GenBank accession no. NM_198965.1), variant 2 (PTHrP-V2, NM_002820.2), variant 3 (PTHrP-V3, NM_198964.1) and variant 4 (PTHrP-V4, NM_198966.1). The full-length cDNAs of *PTHrP-V1*, *V2*, *V3* and *V4* consist of 1331, 1881, 1862 and 1312 nucleotides that encode 177, 175, 175 and 177 amino acids, respectively, and consist of 5, 4, 3, and 4 exons, respectively. The V1 variant lacks exon 3, and the V2 variant lacks exon 3 and possesses exon 5b, which is 1,027 bp longer at the 3′ end than exon 5a. The V3 and V4 variants commonly lack exons 1 and 2 and possess exon 3, which is located within intron 2 with a length of 281 bp. The V3 variant further lacks exon 6, and possesses exon 5b and V2 variant. The V4 variant possesses exon 5a and exon 6, indicating that the *PTHrP-V1/V2* and *V3/V4* variants have different promoter regions (Figure 1A). Subsequent real-time RT-PCR analysis confirmed that the *PTHrP-V3* and *V4* splicing variants were predominately upregulated at the transcriptional level in EGR4-overexpressing HEK293T cells compared with mock-transfected cells (Figure 1B). Accordingly, to obtain direct evidence for the upregulation of *PTHrP-V3* and *V4* by EGR4, we first searched for putative EGR DNA binding motifs with the MatInspector program (described above) because it has been reported that the EGR family, including the EGR4 protein, preferentially binds to an EGR consensus motif (5′-GCGG/TGGGCG-3′) [24–27]. We found a potential EGR DNA binding motif within the *PTHrP-V3* and *V4* promoter region (−515 to −499). Subsequently, we examined the transcriptional activity of EGR4 by a luciferase reporter assay using a pGL3 luciferase plasmid containing the EGR4 binding motif in the *PTHrP-V3/V4* promoter. A significant increase in luciferase activity was observed with FLAG-EGR4 transfection compared with the mock control vector in HEK293T cells (Figure 1C). To further investigate whether EGR4 could bind to a potential *PTHrP-V3* and *V4* EGR binding motif, we performed a ChIP assay. The genomic fragment including the potential EGR binding motif (−515 to −499) of *PTHrP-V3* and *V4* was specifically bound by EGR4 protein in products immunoprecipitated with an anti-FLAG antibody, suggesting that EGR4 directly bound to the promoter region of the *PTHrP-V3* and *V4* variants (Figure 1D). Taken together, these findings suggest that the EGR4 might directly upregulate the *PTHrP-V3* and *V4* variants in SCLC cells.

Paracrine effects of PTHrP secreted from EGR4-overexpressing cells

It has been reported that PTHrP protein secreted from cancer cells regulates the expression of the *RANKL*, *IL-6* and *IL-8* genes, which have been implicated as factors that enhance osteoclast formation and bone destruction in malignant diseases [28–30] in osteoblast cells. According to these data and our findings as shown in Figure 1, we hypothesized that PTHrP protein is secreted from EGR4-overexpressing cells. Our results showed that the PTHrP protein concentration was significantly increased in media conditioned from EGR4-overexpressing HEK293T cells (14.43 ± 1.04 pmol/L) compared with conditioned media from mock-transfected cells (11.83 ± 0.15 pmol/L, $P<0.05$; Figure 2A).

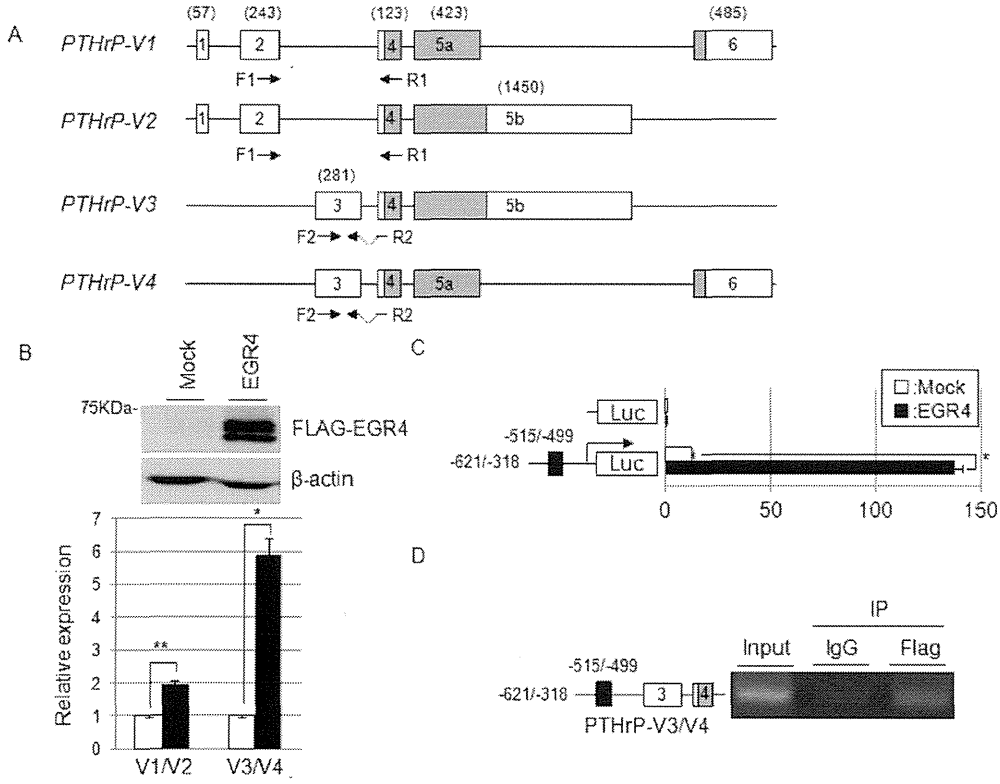

Figure 1. EGR4 directly transactivates specific splice variants of the *PTHrP* gene. A: Genomic structures of the four splice variants of *PTHrP*. The gray and white boxes indicate coding and non-coding regions, respectively. The arrows indicate the primer sets used to perform RT-PCR for each transcript. The numbers in parentheses indicate the length of each exon. B: Upper panel: western blot analysis of HEK293T cells expressing exogenous FLAG-tagged EGR4 (FLAG-EGR4) or cells transfected with the mock vector. Lower panel: real-time RT-PCR analysis of *PTHrP* splice variants (*V1/V2* and *V3/V4*) in EGR4-overexpressing HEK293T cells. C: Luciferase assay of the *PTHrP-V3* and *-V4* (*V3/V4*) promoter regions (n = 2, *$P<0.05$). This experiment was performed using a part of the lysates from cells expressing exogenous FLAG-EGR4 or those transfected with the mock vector used in B. D: ChIP assay of the *PTHrP-V3/V4* promoter region. ChIP assays were used to determine direct EGR4 binding to the *PTHrP-V3/V4* promoter. The PCR product was from −620 to −318 of the region upstream of the 5′ end of exon 3 of *PTHrP-V3/V4*, which was designated as the +1 position.
doi:10.1371/journal.pone.0113606.g001

Next, we evaluated the paracrine effects of conditioned medium from EGR4-overexpressing HEK293T cells on osteoblast cells. As shown in Figure 2B, we transferred conditioned medium from HEK293T cells transfected with the FLAG-EGR4 construct to MC3T3-E1 murine osteoblast cells and then performed real-time PCR to examine the effects of the conditioned medium on the expression level of the *RANKL*, *IL-6* and *IL-8* genes. All three genes were significantly upregulated in osteoblast cells treated with conditioned medium from HEK293T cells ectopically expressing FLAG-EGR4 compared with mock-transfected cells (Figure 2C). Collectively, these findings suggest that the increase in PTHrP secretion from EGR4-overexpressing cells may enhance the expression of the *RANKL*, *IL-6* and *IL-8* genes in osteoblast cells.

Effect of *EGR4* on cell growth

We first examined *EGR4* expression in SCLC cells by semi-quantitative RT-PCR and found that *EGR4* was highly expressed in SBC-3, SBC-5 and NCI-H1048 cells but not in the small airway epithelial cell line SAEC (Figure 3A). Next, to assess whether EGR4 is essential for the growth of SBC-5 cells, we used an RNA interference approach with two different siRNA oligonucleotides. Real-time PCR analysis showed that *EGR4*-specific siRNAs (siEGR4-1 and siEGR4-2) significantly suppressed the expression of EGR4 compared with siEGFP as a control (Figure 3B). MTT assay showed that the introduction of siEGR4s (siEGR4-1 and siEGR4-2) significantly suppressed the growth of SBC-5 cells (Figure 3C), which is in accordance with the EGR4 knockdown results. We also confirmed significant growth inhibitory effects of *EGR4* knockdown in other SCLC cell lines SBC-3 and NCI-H1048 overexpressing *EGR4* (Figure S1). To further confirm the growth promoting effect of *EGR4*, FLAG-EGR4 construct or mock vector was transiently transfected into NIH3T3 cells, and MTT assay was performed as described above. As shown in Figure 3D, FLAG-EGR4-transfected cells grew significantly faster than those transfected with mock vector. These findings suggest that overexpression of *EGR4* might be involved in the growth of SCLC cells.

Identification of *EGR4* target genes

To obtain further insight into the biological role of *EGR4* on cell growth, we attempted to identify downstream genes specifically regulated by EGR4 in SCLC cells. siEGR4 or siEGFP (control siRNA) was transfected into SBC-5 cells in which *EGR4* was highly expressed (Figure 3A), and alterations in gene expression at two time points were monitored by DNA microarray analysis. To identify the genes putatively regulated by EGR4, we selected genes with the following two criteria: (i) expression level was decreased by more than two-fold at 48 and 72 h in cells

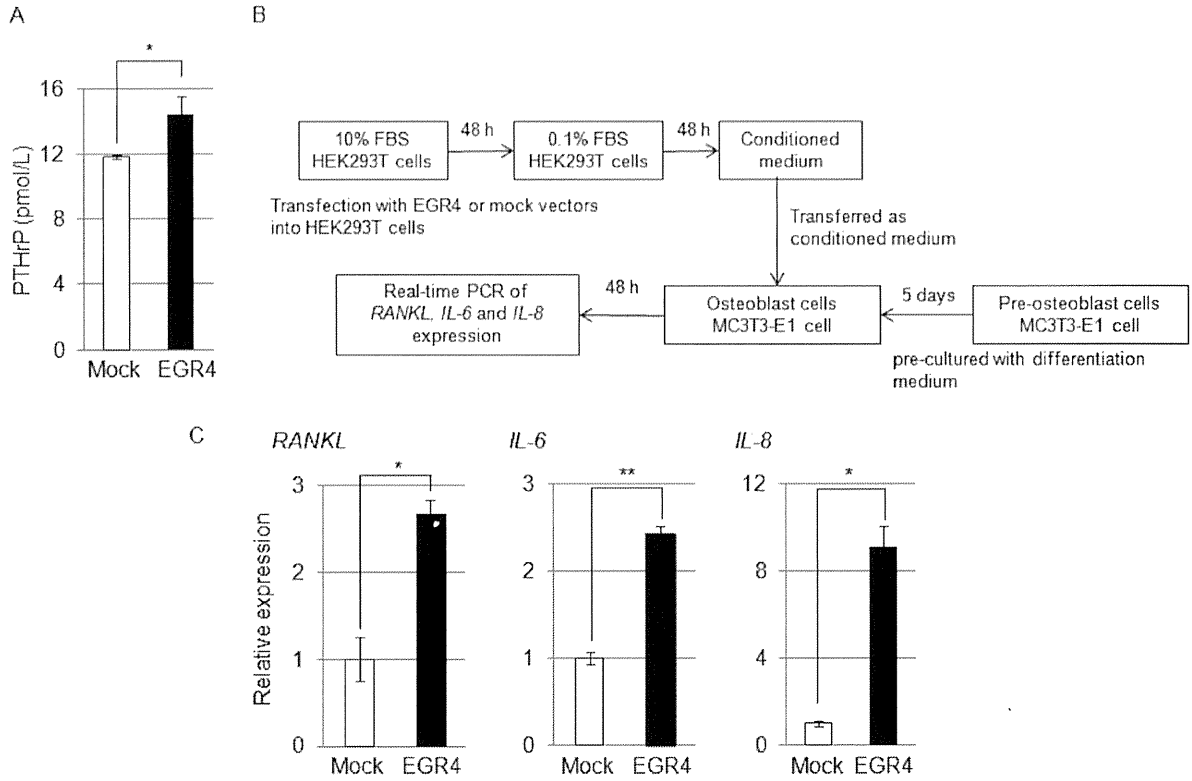

Figure 2. PTHrP secretion leads to transactivation of specific *PTHrP* splice variants. A: Secretion of the PTHrP protein from EGR4-overexpressing HEK293T cells (n = 3, *$P<0.05$). B: Measurement scheme for the paracrine effects of conditioned media from EGR4-overexpressing cells. C: Real-time PCR analysis of the paracrine effects on the expression of the *RANKL*, *IL-6* and *IL-8* genes when medium from EGR4-overexpressing HEK293T cells was cultured with mouse MC3T3-E1 osteoblast cells (n = 2, *, $P<0.05$, **, $P<0.01$).
doi:10.1371/journal.pone.0113606.g002

transfected with siEGR4 compared with cells transfected with the control siEGFP, and (ii) a putative EGR binding motif was predicted to exist within 500 bp of the transcription start site by the MatInspector program (described above). We identified 13 genes that were downregulated upon knockdown of EGR4 expression (Table S5). Real-time PCR analysis confirmed that seven transcripts were significantly downregulated at both time points in EGR4-knockdown cells (Figure 4A). Subsequently, we also evaluated the upregulation of these genes upon exogenous EGR4 expression in HEK293T cells and ultimately selected four EGR4 candidate target genes, including distal-less homeobox 5 (*DLX5*), synaptopodin (*SYNPO*), sterile alpha motif domain containing 5 (*SAMD5*), and RAB15, a member of the RAS oncogene family (*RAB15*), which were significantly upregulated by *EGR4* overexpression (Figure 4B). We confirmed significant downregulation of *DLX5*, *SYNPO* and *SAMD5* genes by *EGR4* knockdown in SBC-3 cells (Figure S2).

To obtain direct evidence for the transactivation of four EGR4 candidate target genes, we measured the transcriptional activity of EGR4 by a luciferase reporter assay. FLAG-EGR4-tranfected cells had significantly higher luciferase activity than mock-transfected cells (Figure 4C). Next, we investigated the recruitment of EGR4 to each EGR4-binding site by ChIP assay. EGR4 was shown to bind to the predicted EGR-binding motif within the promoter regions of all target genes (Figure 4D). These results suggest that EGR4 directly transactivates *SAMD5*, *RAB15*, *SYNPO* and *DLX5*. Subsequently, we investigated the biological role of the four EGR4 target genes in the proliferation of SCLC cells. Introduction of the siRNAs into SBC-5, SBC-3 and NCI-H1048 cells resulted in a significant reduction in the expression of the target genes accompanied by significant suppression of cell proliferation (Figure 5A–D, Figure S3), suggesting that these genes are also likely to play a crucial role in the proliferation of SCLC cells via EGR4 transcriptional activation.

Discussion

In this study, our aim was to identify and characterize molecules or pathways potentially involved in cancer metastasis, particularly bone metastasis. Through a genome-wide transcriptomic analysis of the organ-preferential metastasis of human SCLC cells in mice, we found that *EGR4*, a member of a family of four related zinc-finger Cys_2-His_2 type proteins (*EGR1* to *EGR4*), is significantly upregulated in bone metastatic tumors compared with other organs i.e., the lung, kidney and liver [7]. EGR4 was initially identified as a zinc-finger transcription factor immediately induced by mitogenic stimulation in T lymphocytes and fibroblasts [31]. Gene targeting studies in mice have shown that EGR4 regulates several critical genes involved in the early stages of meiosis and plays an indispensable role in male murine fertility [11,12]. Furthermore, it has been reported that EGR4 binds to nuclear factor activated T cells (NFAT) or nuclear factor kappa B (NFκB) to enhance the transcription of downstream genes encoding inflammatory cytokines, such as IL-2, TNF-α and ICAM-1 [32,33]. A previous report described that the expression level of

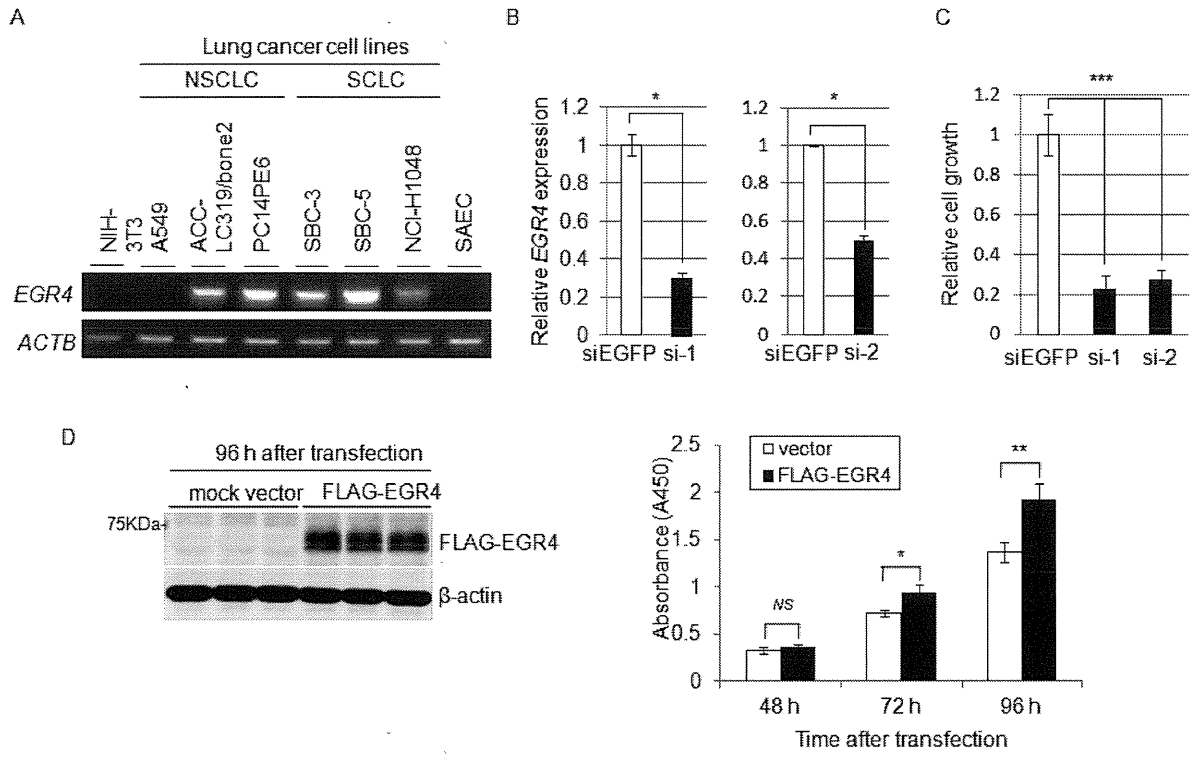

Figure 3. Effects of *EGR4* gene on cell growth. A: Expression of *EGR4* in SCLC and NSCLC cell lines was determined by semi-quantitative RT-PCR. B: Effects of *EGR4* knockdown on cell proliferation in SBC-5 cells. Real-time PCR of *EGR4* in siEGFP- or siEGR4 (siEGR4-1, siEGR4-2)-treated cells at 5 days after siRNA treatment (n = 2, *$P<0.05$). *ACTB* was used as a quantitative control for real-time RT-PCR. C: Cell proliferation was determined by MTT assay at 5 days after siRNA treatment (n = 3, ***$P<0.005$). (si-1; siEGR4-1, si-2; siEGR4-2). D: Growth-promoting effect of exogenous EGR4 on NIH3T3 cells (*$P<0.05$, **$P<0.01$, *NS*, no significance). Western blot analysis was performed at 96 h after transfection (left panel). MTT assay was performed at 48, 72 and 96 h after transfection with FLAG-EGR4 (black) or mock vector (white) (right panel). These experiments were performed in triplicate.
doi:10.1371/journal.pone.0113606.g003

PTHrP, a potent activator of osteoclastic bone resorption, in bone metastases tends to be higher than that in metastases to the kidneys, livers, and lungs using a genome-wide transcriptomics of human SCLC cells in mice [7]. Accordingly, in this study, we focused on *PTHrP*, a potent activator of osteoclastic bone resorption, as an EGR4-downstream gene to clarify the pathophysiological role of EGR4 as a transcription factor in SCLC bone metastases.

PTHrP is known to be a key mediator of humoral hypercalcemia malignancies and osteolytic lung cancer metastases [22,23,34]. Approximately 80% of patients with solid tumors and hypercalcemia have increased PTHrP concentrations in their plasma [35]. It has been reported that PTHrP protein secreted from cancer cells regulates the expression of the *RANKL*, *IL-6* and *IL-8* genes, which have been implicated as factors that enhance osteoclast formation and bone destruction in malignant diseases [28–30] in osteoblast cells. We found that EGR4 directly transactivates specific variants (*V3* and *V4*) of the *PTHrP* gene, thereby possibly promoting the secretion of the PTHrP protein in EGR4-overexpressing cells, resulting in subsequent transactivation of the *RANKL*, *IL-6* and *IL-8* genes via paracrine action of PTHrP. RANKL is known to bind the RANK receptor on osteoclast precursors and induce osteoclast formation. IL-6 and IL-8 have also been reported to be important for osteoclastogenesis and osteoclast activation, respectively [30]. Therefore, these findings suggest that induction of PTHrP by EGR4 overexpression may be responsible for the bone metastasis of SCLC lung cancer cells. However, we found that *PTHrP* gene expression was not reduced by EGR4 knockdown in SBC5 cells (data not shown). A possible reason for this result is that several factors are involved in the regulation of *PTHrP* expression in addition to the EGR4 transcription factor. For example, EGR4 is reported to functionally cooperate with NF-κB and NFAT and induce the expression of cytokine genes [32,33]. Indian hedgehog and TGF-β have also been reported to stimulate perichondrial and breast cancer production, respectively [36,37]. Moreover, miR-33a has been reported to repress the PTHrP-mediated expression of *PTHrP* in NSCLC [38], and knockdown of zinc-finger E-box binding homeobox 1 (ZEB1), a transcriptional repressor, reduces PTHrP secretion in SCLC [39]. Therefore, it is necessary to further explore the mechanism of *PTHrP* transactivation via endogenous EGR4 expression in SBC-5 cells in greater detail.

Notably, we showed that depletion of *EGR4* by siRNA led to a significant reduction in cell proliferation in SBC-5, SBC-3 and NCI-H1048 cells, and that EGR4 transactivated a set of genes possibly related to lung cancer cell growth including four EGR4-downstream genes, *DLX5*, *RAB15*, *SAMD5* and *SYNPO*. Knockdown of the expression of these genes by siRNA led to a significant reduction in cell growth in SCLC cells, suggesting that these genes are involved in the growth of SCLC lung cancer cells. It has been reported that *DLX-5* overexpression in lung cancer cells is associated with tumor size and predictive of poor prognosis and NSCLC cell proliferation [20]. RAB15 was originally identified as a brain-tissue specific RAB protein within the RAB

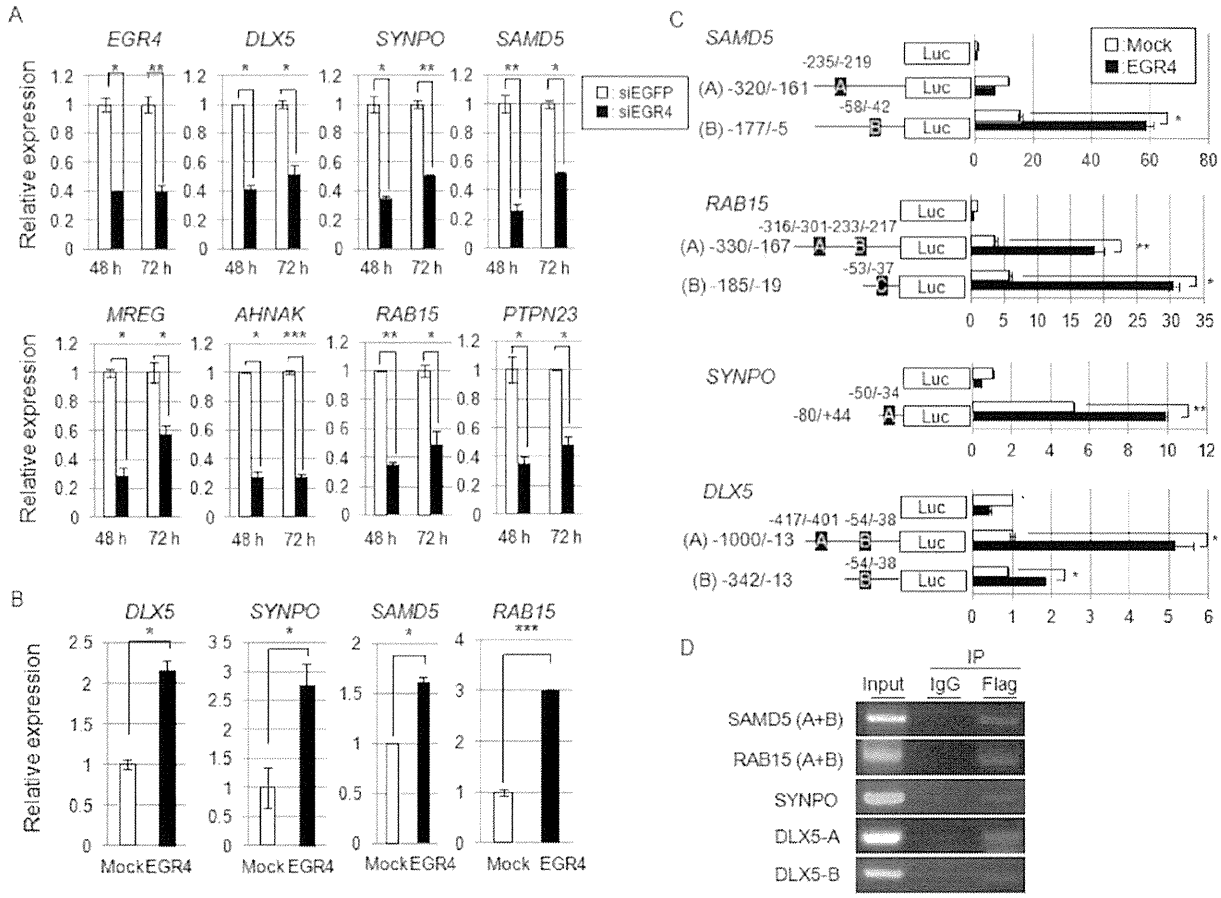

Figure 4. Identification of EGR4-downstream genes involved in the proliferation of SCLC cells. A: Real-time PCR of *EGR4* and seven downstream genes (*DLX5, SYNPO, SAMD5, MREG, AHNAK, RAB15*, and *PTPN23*) in siEGFP- or siEGR4-treated SBC-5 cells (n = 2, *, $P<0.05$, **, $P<0.01$, ***, $P<0.005$). B: Real-time PCR of the *DLX5, SYNPO, SAMD5*, and *RAB15* genes in mock- or EGR4-overexpressing HEK293T cells (n = 2, *, $P<0.05$, ***, $P<0.005$). This experiment was performed using total RNA from cells expressing exogenous FLAG-tagged EGR4 (FLAG-EGR4) or those transfected with the mock vector used in Figure 1B. C: Luciferase assay of the *SAMD5, RAB15, SYNPO* and *DLX5* genes. (n = 2, *, $P<0.05$, **, $P<0.01$). D: ChIP assays were used to determine the direct binding of EGR4 to the promoters of the *SAMD5, RAB15, SYNPO* and *DLX5* genes.
doi:10.1371/journal.pone.0113606.g004

family of small G proteins that regulates the endocytic recycling pathway [40] and is associated with the retinoic acid-induced differentiation of neuroblastoma cells [41]. *SAMD5* has been reported to be one of 24 discriminating genes with an expression level that significantly differs between responders and nonresponders to chemoradiotherapy in rectal cancer [42]. SYNPO has been reported to be an actin-binding protein that functions in actin dynamics, cell migration, and tumor suppression [43] and is exclusively expressed in highly dynamic cell compartments such as kidney podocyte foot processes [44]. Although the precise function of these genes in lung carcinogenesis remains largely unknown, our findings suggest that EGR4 may be a pivotal regulator that selectively activates the transcription of several target genes in lung cancer cells.

In addition, we demonstrated that *EGR4* was highly expressed in NSCLC and SCLC cell lines (Figure 3A). In addition, analysis of publicly available RNAseq data sets from The Cancer Genome Atlas (TCGA) revealed that *EGR4* was up-regulated (more than 2-fold) in 17 of 39 lung adenocarcinoma cases (Figure S4A), and in 19 of 46 squamous cell carcinoma (SCC) cases (Figure S4B) compared with their corresponding normal lung. Furthermore, we found that knockdown of *EGR4* by siRNA suppressed the proliferation of PC14PE6 NSCLC cells (Figure S5), but did not find the inhibitory effects of EGR4 knockdown on its downstream genes, *SAMD5*, *RAB15*, *SYNPO* and *DLX5* expression in PC14PE6 cells (data not shown). These findings suggest the possibility that EGR4 may play different roles in NSCLC cell growth. Therefore, it is necessary to further explore the mechanism of *EGR4* transactivation in NSCLC cells.

In summary, we demonstrated that EGR4 directly transactivates specific variants (*V3* and *V4*) of the *PTHrP* gene, thereby possibly enhancing secretion of the PTHrP protein in EGR4-overexpressing cells, resulting in subsequent transactivation of the *RANKL*, *IL-6* and *IL-8* genes via paracrine action of the PTHrP protein, a mediator of osteolytic bone metastasis (Figure 2). Moreover, EGR4 also transactivates *SAMD5*, *RAB15*, *SYNPO* and *DLX5*, which are involved in the proliferation of SCLC cells. Collectively, our findings suggest that EGR4 is likely to play an important role for the promotion of SCLC growth through the up-regulation of its downstream genes, and it could be a novel therapeutic target for the development of anticancer drugs.

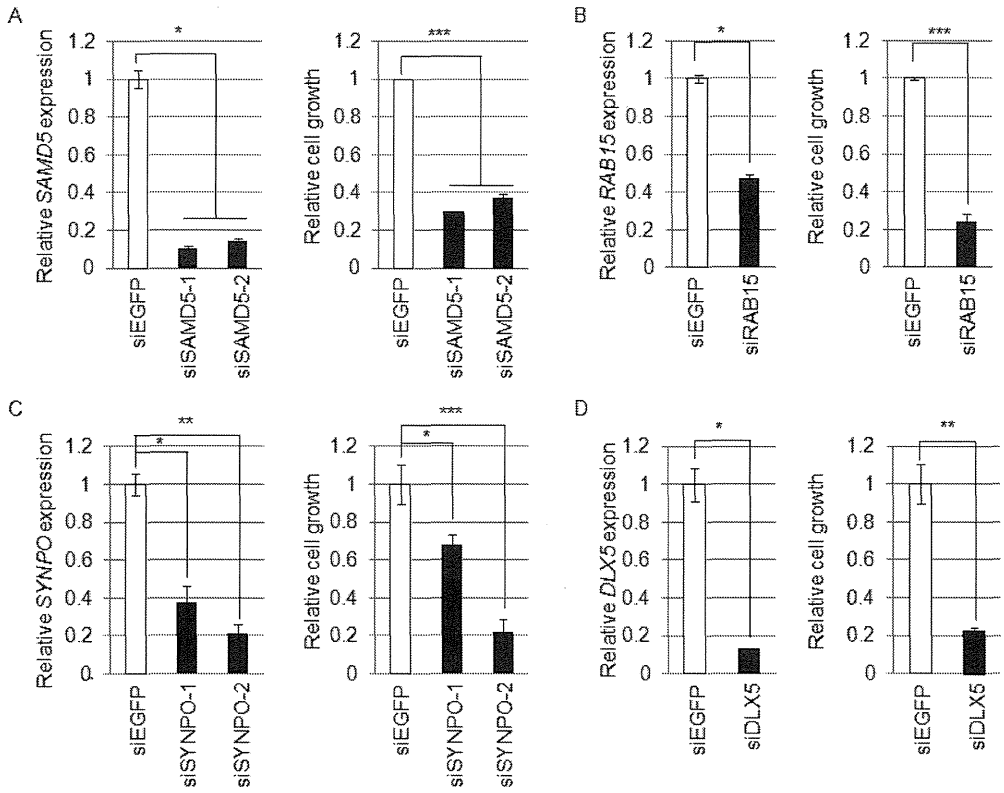

Figure 5. *EGR4* downstream target genes regulate the cell proliferation of SBC-5 cells. Effects of the *EGR4* downstream genes *SAMD5* (A), *RAB15* (B), *SYNPO* (C) and *DLX5* (D) on cell proliferation were determined by siRNA knockdown in SBC-5 cells. The left panel shows the real-time PCR results for target genes in siRNA-treated cells (n = 2). The right panel shows results from cell proliferation analyses as measured by MTT assay (*SAMD5* and *RAB15*: n = 2, *DLX5* and *SYNPO*: n = 3, *, $P<0.05$, **, $P<0.01$, ***, $P<0.005$).
doi:10.1371/journal.pone.0113606.g005

Supporting Information

Figure S1 Effects of *EGR4* gene on SBC-3 and NCI-H1048 cell growth. Effects of *EGR4* knockdown on cell proliferation in SBC-3 and NCI-H1048 cells. Real-time PCR of *EGR4* in siEGFP- or siEGR4 (siEGR4-1, siEGR4-2)-treated SBC-3 cells (A) and NCI-H1048-cells (C) at 5 days after siRNA treatment (n = 2, *$P<0.05$, **, $P<0.01$). *ACTB* was used as a quantitative control for real-time RT-PCR. Cell proliferation of SBC-3 (B) and NCI-H1048 (D) was determined by MTT assay at 5 days after siRNA treatment (n = 3, *$P<0.05$, **, $P<0.01$, ***$P<0.005$). (si-1; siEGR4-1, si-2; siEGR4-2).
(TIFF)

Figure S2 Expression of EGR4-downstream genes in siEGR4-treated SBC-3 cells. Real-time PCR of *EGR4* and 3 downstream genes (*DLX5*, *SYNPO* and *SAMD5*) in SBC-3 cells treated with siEGFP or siEGR4 for 48 h (n = 2, *, $P<0.05$, **, $P<0.01$, ***, $P<0.005$).
(TIFF)

Figure S3 *EGR4*-downstream target genes regulate the cell proliferation of SBC-3 and NCI-H1048 cells. Effects of the *EGR4* downstream genes on cell proliferation were determined in SBC-3 (A–C) and NCI-H1048 cells (D, E). The left panel shows the real-time PCR results for *EGR4*-downstream genes in siRNA-treated cells (n = 2). The right panel shows results from cell proliferation analyses as measured by MTT assay (n = 3, *, $P<0.05$, **, $P<0.01$, ***, $P<0.005$).
(TIF)

Figure S4 Overexpression of *EGR4* in lung cancers. The cases overexpressing *EGR4* (>2 fold compared with the adjacent normal lung) are indicated as black bars in adenocarcinoma (A) and squamous cell carcinoma (SCC) (B).
(TIFF)

Figure S5 Effect of *EGR4* on cell proliferation in PC14PE6 cells. Knockdown of *EGR4* at the mRNA level was analyzed by real-time PCR (n = 2, **$P<0.01$, ***$P<0.005$). Cell proliferation was determined by an MTT assay at 4 days after siRNA treatment (n = 3, ***, $P<0.005$).
(TIFF)

Table S1 Primer sequences for plasmid construction.
(DOCX)

Table S2 Primer sequences for real time PCR or RT-PCR.
(DOCX)

Table S3 Primer sequences for ChIP assay.
(DOCX)

Table S4 siRNA sequences.
(DOCX)

Table S5 Putative downstream EGR4 target genes identified by microarray analysis.
(DOCX)

Acknowledgments

We thank Dr. Tomoya Fukawa (The University of Tokushima) for helpful discussions and Ms. Hinako Koseki and Ms. Hitomi Kawakami for technical assistance. This study was supported by future advanced research from the University of Tokushima.

Author Contributions

Conceived and designed the experiments: TK. Performed the experiments: TM LTD TY MK KD. Analyzed the data: TM LTD TY MK KD. Contributed reagents/materials/analysis tools: SS YN. Wrote the paper: TK TM LTD MK.

References

1. Jemal A, Bray F, Center MM, Ferlay J, Ward E, et al. (2011) Global cancer statistics. CA Cancer J Clin 61: 69–90.
2. Nakazawa K, Kurishima K, Tamura T, Kagohashi K, Ishikawa H, et al. (2012) Specific organ metastases and survival in small cell lung cancer. Oncol Lett 4: 617–620.
3. Al Husaini H, Wheatley-Price P, Clemons M, Shepherd FA (2009) Prevention and management of bone metastases in lung cancer: a review. J Thorac Oncol 4: 251–259.
4. Mundy GR (2002) Metastasis to bone: causes, consequences and therapeutic opportunities. Nat Rev Cancer 2: 584–593.
5. Roodman GD (2004) Mechanisms of bone metastasis. N Engl J Med 350: 1655–1664.
6. Papachristou DJ, Basdra EK, Papavassiliou AG (2012) Bone metastases: molecular mechanisms and novel therapeutic interventions. Med Res Rev 32: 611–636.
7. Kakiuchi S, Daigo Y, Tsunoda T, Yano S, Sone S, et al. (2003) Genome-wide analysis of organ-preferential metastasis of human small cell lung cancer in mice. Mol Cancer Res 1: 485–499.
8. Poirier R, Cheval H, Mailhes C, Garel S, Charnay P, et al. (2008) Distinct functions of egr gene family members in cognitive processes. Front Neurosci 2: 47–55.
9. Müller HJ, Skerka C, Bialonski A, Zipfel PF (1991) Clone pAT 133 identifies a gene that encodes another human member of a class of growth factor-induced genes with almost identical zinc-finger domains. Proc Natl Acad Sci U S A 88: 10079–10083.
10. Crosby SD, Puetz JJ, Simburger KS, Fahrner TJ, Milbrandt J (1991) The early response gene NGFI-C encodes a zinc finger transcriptional activator and is a member of the GCGGGGGCG (GSG) element-binding protein family. Mol Cell Biol 11: 3835–3841.
11. Tourtellotte WG, Nagarajan R, Auyeung A, Mueller C, Milbrandt J (1999) Infertility associated with incomplete spermatogenic arrest and oligozoospermia in Egr4-deficient mice. Development 126: 5061–5071.
12. Tourtellotte WG, Nagarajan R, Bartke A, Milbrandt J (2000) Functional compensation by Egr4 in Egr-1dependent luteinizing hormone regulation and Leydig cell steroidogenesis. Mol Cell Biol 20: 5261–5268.
13. Crosby SD, Veile RA, Donis-Keller H, Baraban JM, Bhat RV, et al. (1992) Neural-specific expression, genomic structure, and chromosomal localization of the gene encoding the zinc-finger transcription factor NGFI-C. Proc Natl Acad Sci U S A 89: 4739–4743.
14. Ludwig A, Uvarov P, Soni S, Thomas-Crusells J, Airaksinen MS, et al. (2011) Early growth response 4 mediates BDNF induction of potassium chloride cotransporter 2 transcription. J Neurosci 31: 644–649.
15. Kiura K, Watarai S, Shibayama T, Ohnoshi T, Kimura I, et al. (1993) Inhibitory effects of cholera toxin on in vitro growth of human lung cancer cell lines. Anticancer Drug Des 8: 417–428.
16. Yano S, Nokihara H, Hanibuchi M, Parajuli P, Shinohara T, et al. (1997) Model of malignant pleural effusion of human lung adenocarcinoma in SCID mice. Oncol Res 9: 573–579.
17. Otsuka S, Hanibuchi M, Ikuta K, Yano S, Goto H, et al. (2009) A bone metastasis model with osteolytic and osteoblastic properties of human lung cancer ACC-LC-319/bone2 in natural killer cell-depleted severe combined immunodeficient mice. Oncol Res 17: 581–591.
18. Matsuo T, Komatsu M, Yoshimaru T, Kiyotani K, Miyoshi Y, et al. (2014) Involvement of B3GALNT2 overexpression in the cell growth of breast cancer. Int J Oncol 44: 427–434.
19. Yoshimaru T, Komatsu M, Matsuo T, Chen YA, Murakami Y, et al. (2013) Targeting BIG3-PHB2 interaction to overcome tamoxifen resistance in breast cancer cells. Nat Commun 4: 2443.
20. Kato T, Sato N, Takano A, Miyamoto M, Nishimura H, et al. (2008) Activation of placenta-specific transcription factor distal-less homeobox 5 predicts clinical outcome in primary lung cancer patients. Clin Cancer Res 14: 2363–2370.
21. Dat le T, Matsuo T, Yoshimaru T, Kakiuchi S, Goto H, et al. (2012) Identification of genes potentially involved in bone metastasis by genome-wide gene expression profile analysis of non-small cell lung cancer in mice. Int J Oncol 40: 1455–1469.
22. Yamada T, Muguruma H, Yano S, Ikuta K, Ogino H, et al. (2009) Intensification therapy with anti-parathyroid hormone-related protein antibody plus zoledronic acid for bone metastases of small cell lung cancer cells in severe combined immunodeficient mice. Mol Cancer Ther 8: 119–126.
23. Miki T, Yano S, Hanibuchi M, Kanematsu T, Muguruma H, et al. (2004) Parathyroid hormone-related protein (PTHrP) is responsible for production of bone metastasis, but not visceral metastasis, by human small cell lung cancer SBC-5 cells in natural killer cell-depleted SCID mice. Int J Cancer 108: 511–515.
24. Christy B, Nathans D (1989) DNA binding site of the growth factor-inducible protein Zif268. Proc Natl Acad Sci USA 86: 8737–8741.
25. Chavrier P, Vesque C, Galliot B, Vigneron M, Dollé P, et al. (1990) The segment-specific gene Krox-20 encodes a transcription factor with binding sites in the promoter region of the Hox-1.4 gene. EMBO J 9: 1209–1218.
26. Lemaire P, Vesque C, Schmitt J, Stunnenberg H, Frank R, et al. (1990) The serum-inducible mouse gene Krox-24 encodes a sequence-specific transcriptional activator. Mol Cell Biol 10: 3456–3467.
27. Swirnoff AH, Milbrandt J (1995) DNA-binding specificity of NGFI-A and related zinc finger transcription factors. Mol Cell Biol 15: 2275–2287.
28. Sone S, Yano S (2007) Molecular pathogenesis and its therapeutic modalities of lung cancer metastasis to bone. Cancer Metastasis Rev 26: 685–689.
29. Chen YC, Sosnoski DM, Mastro AM (2010) Breast cancer metastasis to the bone: mechanisms of bone loss. Breast Cancer Res 12: 215.
30. Kozlow W, Guise TA (2005) Breast cancer metastasis to bone: mechanisms of osteolysis and implications for therapy. J Mammary Gland Biol Neoplasia 10: 169–180.
31. Skerka C, Decker EL, Zipfel PF (1995) A regulatory element in the human interleukin 2 gene promoter is a binding site for the zinc finger proteins Sp1 and EGR-1. J Biol Chem 270: 22500–22506.
32. Decker EL, Nehmann N, Kampen E, Eibel H, Zipfel PF, et al. (2003) Early growth response proteins (EGR) and nuclear factors of activated T cells (NFAT) form heterodimers and regulate proinflammatory cytokine gene expression. Nucleic Acids Res 31: 911–921.
33. Wieland GD, Nehmann N, Müller D, Eibel H, Siebenlist U, et al. (2005) Early growth response proteins EGR-4 and EGR-3 interact with immune inflammatory mediators NF-kappaB p50 and p65. J Cell Sci 118: 3203–3212.
34. Moseley JM, Kubota M, Diefenbach-Jagger H, Wettenhall RE, Kemp BE, et al. (1987) Parathyroid hormone-related protein purified from a human lung cancer cell line. Proc Natl Acad Sci USA 84: 5048–5052.
35. Burtis WJ, Brady TG, Orloff JJ, Ersbak JB, Warrell RP Jr, et al. (1990) Immunochemical characterization of circulating parathyroid hormone-related protein in patients with humoral hypercalcemia of cancer. N Engl J Med 322: 1106–1112.
36. Vortkamp A, Lee K, Lanske B, Segre GV, Kronenberg HM, et al. (1996) Regulation of rate of cartilage differentiation by Indian hedgehog and PTH-related protein. Science 273: 613–622.
37. Johnson RW, Nguyen MP, Padalecki SS, Grubbs BG, Merkel AR, et al. (2011) TGF-beta promotion of Gli2-induced expression of parathyroid hormone-related protein, an important osteolytic factor in bone metastasis, is independent of canonical Hedgehog signaling. Cancer Res 71: 822–831.
38. Kuo PL, Liao SH, Hung JY, Huang MS, Hsu YL (2013) MicroRNA-33a functions as a bone metastasis suppressor in lung cancer by targeting parathyroid hormone related protein. Biochim Biophys Acta 1830: 3756–3766.
39. Liu Y, Zhang N, Wang Y, Xu M, Liu N, et al. (2012) Zinc finger E-box binding homeobox 1 promotes invasion and bone metastasis of small cell lung cancer in vitro and in vivo. Cancer Sci 103: 1420–1428.
40. Zuk PA, Elferink LA (2000) Rab15 differentially regulates early endocytic trafficking. J Biol Chem 275: 26754–26764.
41. Nishimura N1, Van Huyen Pham T, Hartomo TB, Lee MJ, Hasegawa D, et al. (2011) Rab15 expression correlates with retinoic acid-induced differentiation of neuroblastoma cells. Oncol Rep 26: 145–151.
42. Watanabe T, Kobunai T, Akiyoshi T, Matsuda K, Ishihara S, et al. (2014) Prediction of response to preoperative chemoradiotherapy in rectal cancer by using reverse transcriptase polymerase chain reaction analysis of four genes. Dis Colon Rectum 57: 23–31.
43. Asanuma K, Yanagida-Asanuma E, Faul C, Tomino Y, Kim K, et al. (2006) Synaptopodin orchestrates actin organization and cell motility via regulation of RhoA signalling. Nat Cell Biol 8: 485–491.
44. Wong JS, Iorns E, Rheault MN, Ward TM, Rashmi P, et al. (2012) Rescue of tropomyosin deficiency in Drosophila and human cancer cells by synaptopodin reveals a role of tropomyosin α in RhoA stabilization. EMBO J 31: 1028–1040.

Chen et al. BMC Research Notes 2014, 7:435
http://www.biomedcentral.com/1756-0500/7/435

BMC Research Notes

RESEARCH ARTICLE Open Access

Brefeldin A-inhibited guanine nucleotide-exchange protein 3 (BIG3) is predicted to interact with its partner through an ARM-type α-helical structure

Yi-An Chen[1], Yoichi Murakami[1,2], Shandar Ahmad[1], Tetsuro Yoshimaru[3], Toyomasa Katagiri[3] and Kenji Mizuguchi[1*]

Abstract

Background: Brefeldin A-inhibited guanine nucleotide-exchange protein 3 (BIG3) has been identified recently as a novel regulator of estrogen signalling in breast cancer cells. Despite being a potential target for new breast cancer treatment, its amino acid sequence suggests no association with any well-characterized protein family and provides little clues as to its molecular function. In this paper, we predicted the structure, function and interactions of BIG3 using a range of bioinformatic tools.

Results: Homology search results showed that BIG3 had distinct features from its paralogues, BIG1 and BIG2, with a unique region between the two shared domains, Sec7 and DUF1981. Although BIG3 contains Sec7 domain, the lack of the conserved motif and the critical glutamate residue suggested no potential guaninyl-exchange factor (GEF) activity. Fold recognition tools predicted BIG3 to adopt an α-helical repeat structure similar to that of the armadillo (ARM) family. Using state-of-the-art methods, we predicted interaction sites between BIG3 and its partner PHB2.

Conclusions: The combined results of the structure and interaction prediction led to a novel hypothesis that one of the predicted helices of BIG3 might play an important role in binding to PHB2 and thereby preventing its translocation to the nucleus. This hypothesis has been subsequently verified experimentally.

Keywords: Breast cancer, Estrogen receptor-alpha, BIG3, PHB2, Protein-protein interaction, Bioinformatics

Background

Breast cancer is the most common cancer among women worldwide [1]. The majorities of breast cancers are estrogen receptor-alpha (ERα) positive and depend on the hormone estrogen for growth. Estradiol (E2) is known to induce cell proliferation by binding to ERα, resulting in the transcriptional activation of its downstream genes [2,3]. Antagonists to ERα such as tamoxifen can block the effects of E2 on breast cancer cells and thereby interfere with estrogen-induced cell proliferation. Although tamoxifen has been a great success and improves breast cancer survival rates considerably [4-6], a significant proportion of ERα-positive breast cancer is tamoxifen-unresponsive, and tamoxifen-resistant cases have been also reported [7,8]. The mechanism of E2/ERα signalling is not fully understood and a better understanding of the E2/ERα pathway will be essential for more effective and alternate treatments for breast cancer.

Recently, genome-wide profiling of gene expression in breast cancer cells has identified a novel regulator of E2/ERα signalling, brefeldin A-inhibited guanine nucleotide-exchange protein 3 (BIG3). BIG3 has been shown to be over-expressed in breast cancer cells but hardly detectable in normal human tissues [8]. Small-interfering RNA (siRNA)-mediated knockdown of BIG3 was shown to suppress the growth of breast cancer cells significantly [9]. Co-immunoprecipitation and immuno-blotting assays have shown that BIG3 interacts with prohibitin 2 (PHB2), a protein that can repress the activity of ER. PHB2 was shown to be localized mainly in the cytoplasm [10]. When BIG3 is absent, E2 stimulation causes the translocation of PHB2 to the nucleus and results in the suppression of the ERα transcriptional activity. On the other hand, when BIG3 is over-expressed, PHB2

* Correspondence: kenji@nibio.go.jp
[1]National Institute of Biomedical Innovation, 7-6-8 Saito-asagi, Ibaraki city, Osaka 567-0085, Japan
Full list of author information is available at the end of the article

remains in the cytoplasm even with estrogen treatment and it has been shown that the intracellular localization of PHB2 is dependent on its interaction with BIG3 in the cytoplasm. Therefore, the current hypothesis is that BIG3 interacts with PHB2 and traps it in the cytoplasm and thereby prevents its nuclear translocation, resulting in increases in the transcriptional activities of ERα.

This novel mechanism of ERα regulation by BIG3 has the potential to offer molecular details of signalling events in ERα-positive breast cancer cells and can lead to new ways of therapeutic intervention. The progress has been hampered, however, by the lack of information about molecular functions of BIG3. The BIG3 protein consists of 2177 amino acid residues and its sequence suggests no association with any well-characterized protein family and provides little clues as to its molecular function. Although a series of co-immunoprecipitation assays identified residues 86-434 to be responsible for the binding of BIG3 to PHB2, further attempts at narrowing down the binding region or any other biochemical characterization had been unsuccessful until computational predictions, described in this paper, were made and subsequently verified experimentally [10].

In this paper, we describe details of our predictions for the structure, function and interactions of BIG3 using state-of-the-art bioinformatic tools. The prediction of protein interaction sites, supported by consistent fold recognition results, led to a specific hypothesis about the nature of the molecular interactions between BIG3 and PHB2, which was a key to the successful experimental verification studies.

Results and discussion

BIG3 has features distinct from BIG1 and BIG2

The BIG3 protein consists of 2177 amino acids but standard sequence-based tools such as Pfam [11] and SMART [12] identified only two domains, Sec7 (at 592-798) and DUF1981 (at 1246-1303) (Figure 1). The Sec7 domain has been shown to be linked with guanine nucleotide exchange factor (GEF) activity [13,14], although its relevance to the biological function of BIG3 is unclear (see below). DUF1981 is a functionally uncharacterized domain defined in Pfam and it is mostly found in GEF related proteins.

To gain further insights into the structure and function of BIG3, we split its amino acid sequence into three segments based on the Pfam and SMART domain assignments and ran BLAST for each segment against the non-redundant protein (nr) database. The segment before the Sec7 domain and that after the DUF1981

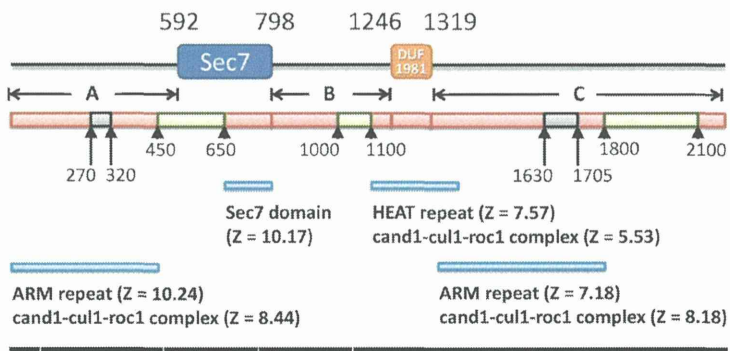

#	Region	Identities	Query Coverage	Hits
A	1 – 592	> 80%	> 85%	BIG3 or BIG3-like from different species
		~ 26%	~ 30%	Mostly BIG2 or BIG2-like from different species
		~ 24%	~ 30%	Mostly BIG1 or BIG1-like from different species
B	798 – 1246	> 85%	100%	BIG3 or BIG3-like from different species
C	1319 - 2177	> 90%	> 99%	BIG3 or BIG3-like from different species
		~ 21%	~ 45%	Mostly BIG2 or BIG2-like from different species
		~ 21%	~ 40%	Mostly BIG1 or BIG1-like from different species

Figure 1 Sequence analysis of BIG3. The locations of the two domains identified by Pfam and SMART are shown at the top. Shown below are the results of secondary structure and disorder predictions: red, α-helical; grey, coil; and green, disorder. The three segments underneath, **A**, **B** and **C**, indicate the query sequences for the BLAST, FUGUE and HHpred searches. The FUGUE hits are shown below and the BLAST results are summarized in the table at the bottom.

domain were found to be conserved both in BIG3 orthologues (annotated as BIG3 in the database) and paralogues (annotated as BIG1 and BIG2). On the other hand, the segment between the Sec7 and DUF1981 domains produced significant hits only to the orthologues (Figure 1). When the sequences of BIG3 and the human BIG family proteins were compared, BIG1 and BIG2 showed 74% identity overall and higher identities in both the Sec7 and DUF1981 domains (90%). However, BIG3 showed only 21% identities to BIG1 and BIG2, with ~30% identity in DUF1981 and no significant similarity (i.e., a BLAST e-value of > 10) found in the Sec7 domain. These observations suggested that BIG3 was the most distinct among its paralogues, with a markedly unique region between the Sec7 and DUF1981 domains.

BIG3, unlike BIG1 and BIG2, potentially lacks GEF activity, despite being annotated to contain the Sec7 domain (based on sequence similarity). Sec7, first discovered in the SEC7 gene product of *S. cerevisiae*, has a central GEF domain for the ADP-ribosylation factor family involved in vesicular transport processes [15-17]. There is a highly conserved motif, FRLPGE, among the Sec7 proteins, with the last glutamate residue essential for GEF activity [18-24]. It has also been shown that the Sec7 domain alone is sufficient for GEF activity [17]. Alignments between BIG3 and known Sec7 proteins (generated with both the sequence-only method CLUSTALW [25] and the structure-based method FUGUE [26]) were stable and unambiguous in a region around the conserved motif, and they showed that BIG3 lacked the conserved motif and critically, the essential glutamate residue (Figure 2). This region is conserved among the BIG3 orthologues, all of which lack the functional motif. This observation suggests that BIG3 is unlikely to be a GEF protein, consistent with a previous demonstration by the GST-GAT pull-down assay [27].

BIG3 is likely to adopt α-helical repeat structures similar to that of the armadillo (ARM) family

We then attempted to predict the structure of BIG3 using more specialized tools. Both POODLE [28,29] and PrDOS [30] predicted BIG3 to adopt largely well-defined three-dimensional structures, except for three intrinsically disordered regions at 450-650, 1000-1100 and 1800-2100. Secondary structure prediction by PSI-PRED suggested that BIG3 predominately consisted of helical structures (Figure 1). No evidence was obtained for any of the predicted helices to be coiled-coil or transmembrane structures. Although no repeats were detected by sequence-based methods (see Methods), fold recognition using FUGUE and HHpred suggested that some parts of BIG3 would consist of ARM (and related) repeats, with statistically significant sores

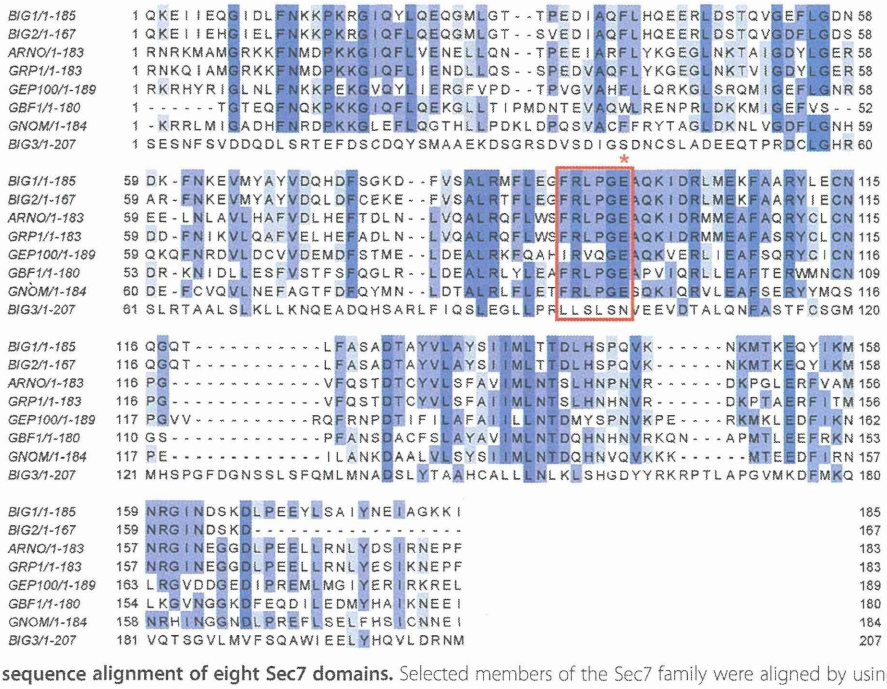

Figure 2 Multiple sequence alignment of eight Sec7 domains. Selected members of the Sec7 family were aligned by using CLUSTALW. (See Methods for the protein names and accessions.) Sequences are coloured by percentage identities: dark purple, >80%; purple, 60% ~ 80%; light purple 40% ~ 60%; white, <40%. The red box shows the conserved motif in Sec7 domain. BIG3 lacks the conserved motif, especially the critical glutamate residue (indicated by the red asterisk).

(FUGUE Z-score > 7, 99% confidence and HHpred probability > 80%; see Figure 1).

Despite the high confidence scores, however, generating alignments proved to be tricky; because of the nature of the α-helical repeats, slightly different alignments were produced for different hits. Figure 3 shows an alignment with the TIP120 protein, the highest scoring hit by FUGUE when queried with residues 86-434 of BIG3. TIP120 is a member of the HEAT repeat family. The HEAT repeat is related to the ARM repeat and sometimes classified as a subgroup of the ARM family. In this alignment, the predicted α-helices generally agree well with the helical positions in the TIP120 structure.

The ARM repeat, first discovered in armadillo gene of Drosophila, is an approximately 40 amino acid long tandem repeat, forming a super-helix of helices. Proteins in the ARM family are known to function in various processes, including cytoskeletal regulation, signalling, tumor suppression and nuclear translocation. It has been proposed that ARM may mediate protein-protein interactions but currently, no typical feature of target proteins is known. Of particular note is that the nuclear transport protein importin, known to recognize nuclear localization signals (NLSs), is a member of the ARM family. Given its predicted structure, BIG3 might also bind to its partners in a similar manner (see below).

Prediction of protein binding sites suggested how BIG3 could possibly inhibit the nuclear translocation of PHB2

To pursue this possibility further, we attempted to predict protein-binding sites on BIG3 using PSIVER [32] and examined the results within the predicted ARM repeats, as these repeats fell within residues 1-250, a region that had been shown experimentally to be responsible for the binding of BIG3 to PHB2 [10].

Figure 3 shows the possible interaction sites on BIG3 predicted by PISVER, combined with the results of FUGUE and PSI-PRED analyses (see Additional file 1 for the raw data). The benchmark results of PSIVER showed that high scoring residues would tend to cluster together near the true interaction sites [32]. Therefore, we highlighted clusters of the highest scoring residues in Figure 3 (yellow background) and considered the residues 157-174 as the most likely interaction site (red background). This region coincides with a predicted α-helix [10], and a helical wheel projection [33] of the residues (Figure 4) shows that the

Figure 3 Predicted structure and interaction sites of BIG3. Results of secondary structure prediction (PSIPRED) and interaction site prediction (PSIVER) were mapped on a structure-based alignment (generated with FUGUE and formatted with JOY [31]) between BIG3 (residues 86-300) and TIP120 (PDB 1u6g, chain C). For the PSIPRED prediction, H stands for α-helices, E for β strands and dash for coil structures. For the PSIVER results, scores greater than 0.39 are labelled with plus (+) signs. Clusters of the highest scoring residues are highlighted with a yellow background and those residues with a score greater than 0.6 are indicated with red plus signs. The helix used for the helical wheel projection (see Figure 4) is indicated with a red background. Structural environments are annotated with JOY, the formatting convention of which is as follows: red, α-helices; blue, β strands; maroon, 3_{10} helices; upper case letters, solvent inaccessible; lower case letters, solvent accessible; bold type, hydrogen bonds to mainchain amides; underlining, hydrogen bonds to mainchain carbonyls; italic, positive mainchain torsion angles φ.

side chains of the residues with locally maximal scores (red plus signs in Figure 3) sit on the same face of the helix. These results have opened a new direction for experimental research, including the construction of BIG3 mutants and the design of an inhibitory peptide. Site-directed mutagenesis showed that substituting Q165, D169 and Q173 (indicated with red plus signs in Figure 3) with alanine reduced the binding affinity to PHB2 dramatically (see Additional file 2: Figure S1 of [10]). The designed peptide, including these PHB2-binding residues, has been shown to inhibit the growth of ERα-positive breast cancer cells both *in vitro* and *in vivo* [10].

Since BIG1 and BIG2, the paralogues of BIG3, share some sequence similarity with BIG3 in their N-terminal portions (region A in Figure 1), we generated a multiple sequence alignment and examined the putative PHB2-binding site, including the three verified binding residues (Figure 5, red box). Because of the general sequence similarity, the alignment in this region was unambiguous and showed that, of the three PHB2-binding residues, only Q165 was conserved among BIG1, BIG2 and BIG3. Since the other two residues have been shown to be critical for PHB2 binding [10], we conclude that BIG1 and BIG2 are unlikely to form a heterodimer with PHB2, although these paralogues may still share some other common functions.

We also predicted protein-binding sites on PHB2. PSIVER predicted a few regions to be possible interacting sites (highlight in Figure 6), one of which (76-88) is close to the predicted NLS. We also used PPiPP, a recently developed neural network-based method for predicting contacting residue pairs given a pair of amino acid sequences [34]. A PPiPP search for interacting pairs between residues 1-300 of BIG3 and PHB2 (full length, 299 amino acid residues) identified R11, R17, M19, Y34, R54, I55, R88, M101 and R289 as the most likely interacting partners of the putative interacting region on BIG3 (157-173, Figure 3, yellow background). By combining this analysis and the prediction results by PSIVER, we found regions 11-21 and 44-57 to be the most likely BIG3-binding site (Figure 6, underlined). PHB2 is known to interact with several other proteins (such as COPG and PTMA), as reported in BIOGRID [35] and PPIview [36]. Whether the predicted region is indeed involved in BIG3-binding is yet to be verified experimentally.

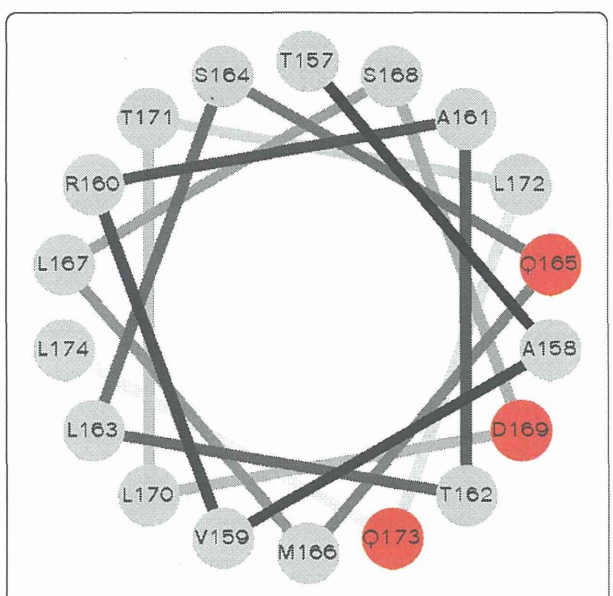

Figure 4 A helical wheel projection of residues 157-174 of BIG3. The residues with the highest predicted interaction scores, Q166, D170 and Q174 (red filled circles), are located on the same face of the helix.

PHB2 is known to be involved in several biological processes and found in different cellular compartments, including the nucleus, mitochondria and cell membrane [37-40]. Although the mechanism of translocation of PHB2 is still unclear, one possibility is that it is mediated by importin (or importin-like proteins), and BIG3 could possibly dislocate importin and interact with PHB2, preventing it from being transported to the nucleus. In light of this hypothesis, it is highly suggestive that BIG3 is predicted to adopt the same fold as that of importin.

Conclusions

Based on the differences in sequence and the lack of conserved motif in the Sec7 domain, BIG3 was shown to have distinct features from its paralogues BIG1 and BIG2. Structural analysis showed that BIG3 would adopt α-helical repeat structures similar to that of the ARM family. Prediction of interaction sites between BIG3 and PHB2 provided a new insight into how BIG3 would interfere the translocation of PHB2 and suggested a specific, testable hypothesis.

Methods

Sequence analysis

Protein sequences of BIG3 [Swiss-Prot:Q5TH69] and PHB2 [Swiss-Prot:Q99623] were retrieved from Uniprot. Pfam (http://pfam.xfam.org/) and SMART (http://smart.embl-heidelberg.de/) searches were performed using their web servers. BLAST was run on the NCBI website (http://www.ncbi.nlm.nih.gov/BLAST/) using default parameters. A multiple sequence alignment of the Sec7 domains of BIG1 [Swiss-Prot:Q9Y6D6], BIG2 [Swiss-Prot:Q9Y6D5], ARNO [Swiss-Prot:Q99418], GBF1 [Swiss-Prot:Q92538], GRP1 [Swiss-Prot:O43739], GNOM [Swiss-Prot:Q42510], GEP100 [Swiss-Prot:Q6ND90] and BIG3 was generated using CLUSTALW and formatted by Jalview [41]. A multiple sequence alignment of the N-terminal portions of BIG3 and its homologues was generated by MAFFT version 7 (http://mafft.cbrc.jp/alignment/server/). The sequences

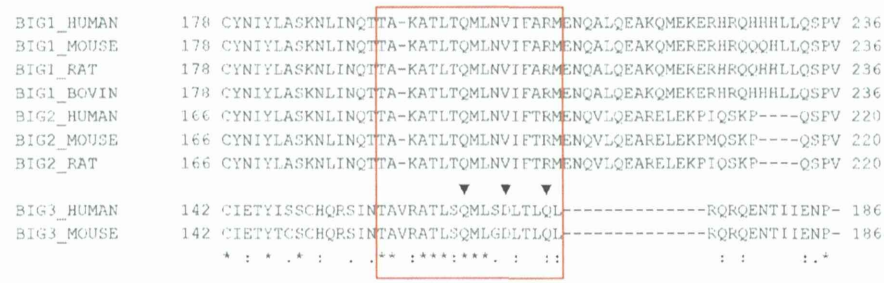

Figure 5 Multiple sequence alignment of BIG3 and its homologues near the putative PHB2-binding site. Multiple sequence alignment of the N-terminal portions (region A in Figure 1) of BIG3 and its homologues was generated by MAFFT (see Additional file 2 for the full alignment). The red box corresponds to the residues in the red background in Figure 3. The verified PHB2-binding residues are indicated with black triangles.

included were human BIG1 [Swiss-Prot:Q9Y6D6] and BIG2 [Swiss-Prot:Q9Y6D5], mouse BIG1 [Swiss-Prot:G3X9K3], BIG2 [Swiss-Prot:A2A5R2] and BIG3 [Swiss-Prot:Q3UGY8], rat BIG1 [Swiss-Prot:D4A631] and BIG2 [Swiss-Prot:Q7TSU1] and bovine BIG1 [Swiss-Prot:O46382].

Structure prediction

Secondary structure was predicted by using a local installation of PSIPRED [42] with the default script. Disordered regions were predicted using both POODLE-L and POODLE-W on the POODLE server (http://mbs.cbrc.jp/poodle/index.html) and PrDOS (http://prdos.hgc.jp/index.html). Coiled-coil was predicted using Paircoil2 (http://groups.csail.mit.edu/cb/paircoil2/) [43] and COILS (http://www.ch.embnet.org/software/COILS_form.html) [44]. Sequence repeats were predicted using REP (http://www.bork.embl.de/~andrade/papers/rep/search.html) [45], HHrep (http://toolkit.tuebingen.mpg.de/hhrep) [46] and REPRO (http://www.ibi.vu.nl/programs/reprowww/) [47]. Fold recognition was performed using FUGUE (http://tardis.nibio.go.jp/fugue/) and HHpred (http://toolkit.tuebingen.mpg.de/hhpred/, with the HMM database of pdb70_18Dec10) [48] using the three segments defined in Figure 1 as queries.

Interaction site prediction

Interaction sites on BIG3 and PHB2 were predicted using PSIVER [32]. The default threshold of 0.390 was used in this study. Interacting pair positions between the two proteins were predicted using PPiPP [34] with default parameters.

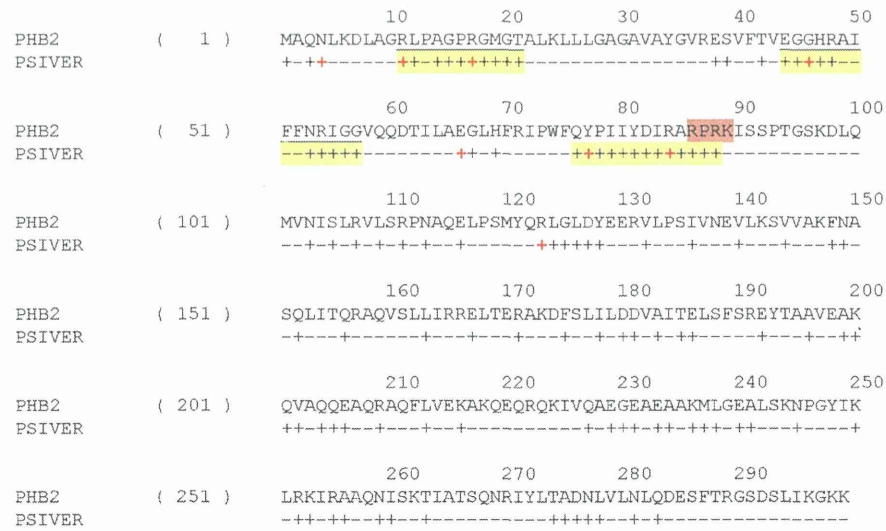

Figure 6 Predicted interaction sites of PHB2. Results of the binding site prediction for PHB2 by PSIVER. Scores greater than 0.39 are labelled with plus (+) signs. Clusters of the highest scoring residues are highlighted with a yellow background and the scores greater than 0.6 are shown in red. The NLS region, residues 86-89, is indicated with a red background. The consensus prediction results for the BIG3 binding site by PSIVER and PPiPP are underlined.

Helical wheel projection

The helical wheel projection was generated by a custom script derived from the original code by Zidovetzki and Armstrong [33].

Additional files

Additional file 1: Detailed prediction results by PSIVER for protein-binding sites on BIG3. The columns represent: record type (always "PRED"), residue position, binary prediction (plus for the raw score above the threshold of 0.39 and minus otherwise), one-letter amino acid code, raw score and z-score, respectively.

Additional file 2: Multiple sequence alignment of the N-terminal portions of BIG3 and its homologues. Multiple sequence alignment of the N-terminal portions (region A in Figure 1) of BIG3 and its homologues by MAFFT.

Competing interests

The authors declare that they have no competing interests.

Authors' contributions

KM conceived and coordinated the study. YAC carried out and summarized the computational analysis. YM and SA participated in the protein-protein interaction prediction. TY and TK participated in the discussion of biological relevance and experimental validation. YAC, YM and KM wrote the manuscript. All authors read and approved the final manuscript.

Acknowledgements

This study was in part supported by the Industrial Technology Research Grant Program in 2007 (Grant Number 07C46056a) from New Energy and Industrial Technology Development Organization (NEDO) of Japan, and also by Grants-in-Aid for Scientific Research from the Ministry of Education, Culture, Sports, Science, and Technology (Grant Numbers 25430186 and 25293079).

Author details

[1]National Institute of Biomedical Innovation, 7-6-8 Saito-asagi, Ibaraki city, Osaka 567-0085, Japan. [2]Graduate School of Information Sciences, Tohoku University, 6-3-09 Aramaki-aza-aoba, Aoba-ku, Sendai city, Miyagi 980-8579, Japan. [3]Division of Genome Medicine, Institute for Genome Research, The University of Tokushima, 3-18-15 Kuramoto-cho, Tokushima 770-8503, Japan.

Received: 23 April 2014 Accepted: 30 June 2014
Published: 6 July 2014

References

1. *GLOBOCAN 2012 v1.0, Cancer Incidence and Mortality Worldwide: IARC CancerBase No. 11.* http://globocan.iarc.fr.
2. Berry DA, Cronin KA, Plevritis SK, Fryback DG, Clarke L, Zelen M, Mandelblatt JS, Yakovlev AY, Habbema JD, Feuer EJ: **Effect of screening and adjuvant therapy on mortality from breast cancer.** *N Engl J Med* 2005, **353**(17):1784–1792.
3. Yager JD, Davidson NE: **Estrogen carcinogenesis in breast cancer.** *N Engl J Med* 2006, **354**(3):270–282.
4. Fisher B, Costantino JP, Wickerham DL, Cecchini RS, Cronin WM, Robidoux A, Bevers TB, Kavanah MT, Atkins JN, Margolese RG, Runowicz CD, James JM, Ford LG, Wolmark N: **Tamoxifen for the prevention of breast cancer: current status of the National Surgical Adjuvant Breast and Bowel Project P-1 study.** *J Natl Cancer Inst* 2005, **97**(22):1652–1662.
5. Johnston SR: **New strategies in estrogen receptor-positive breast cancer.** *Clin Cancer Res Off J Am Assoc Cancer Res* 2010, **16**(7):1979–1987.
6. Jordan VC: **Tamoxifen: a most unlikely pioneering medicine.** *Nat Rev Drug Discov* 2003, **2**(3):205–213.
7. Ring A, Dowsett M: **Mechanisms of tamoxifen resistance.** *Endocrine-related Cancer* 2004, **11**(4):643–658.
8. Wiebe VJ, Osborne CK, Fuqua SA, DeGregorio MW: **Tamoxifen resistance in breast cancer.** *Critical Rev Oncol/hematol* 1993, **14**(3):173–188.
9. Kim JW, Akiyama M, Park JH, Lin ML, Shimo A, Ueki T, Daigo Y, Tsunoda T, Nishidate T, Nakamura Y, Katagiri T: **Activation of an estrogen/estrogen receptor signaling by BIG3 through its inhibitory effect on nuclear transport of PHB2/REA in breast cancer.** *Cancer Sci* 2009, **100**(8):1468–1478.
10. Yoshimaru T, Komatsu M, Matsuo T, Chen YA, Murakami Y, Mizuguchi K, Mizohata E, Inoue T, Akiyama M, Yamaguchi R, Imoto S, Miyano S, Miyoshi Y, Sasa M, Nakamura Y, Katagiri T: **Targeting BIG3-PHB2 interaction to overcome tamoxifen resistance in breast cancer cells.** *Nat Commun* 2013, **4**:2443.
11. Finn RD, Mistry J, Tate J, Coggill P, Heger A, Pollington JE, Gavin OL, Gunasekaran P, Ceric G, Forslund K, Holm L, Sonnhammer EL, Eddy SR, Bateman A: **The Pfam protein families database.** *Nucleic Acids Res* 2010, **38**(Database issue):D211–D222.
12. Letunic I, Doerks T, Bork P: **SMART 6: recent updates and new developments.** *Nucleic Acids Res* 2009, **37**(Database issue):D229–D232.
13. Klarlund JK, Guilherme A, Holik JJ, Virbasius JV, Chawla A, Czech MP: **Signaling by phosphoinositide-3,4,5-trisphosphate through proteins containing pleckstrin and Sec7 homology domains.** *Science* 1997, **275**(5308):1927–1930.
14. Klarlund JK, Rameh LE, Cantley LC, Buxton JM, Holik JJ, Sakelis C, Patki V, Corvera S, Czech MP: **Regulation of GRP1-catalyzed ADP ribosylation factor guanine nucleotide exchange by phosphatidylinositol 3,4,5-trisphosphate.** *J Biol Chem* 1998, **273**(4):1859–1862.
15. Abergel C, Chavrier P, Claverie JM: **Triple association of CDC25-, Dbl- and Sec7-related domains in mammalian guanine-nucleotide-exchange factors.** *Trends Biochem Sci* 1998, **23**(12):472–473.
16. Achstetter T, Franzusoff A, Field C, Schekman R: **SEC7 encodes an unusual, high molecular weight protein required for membrane traffic from the yeast Golgi apparatus.** *J Biol Chem* 1988, **263**(24):11711–11717.
17. Chardin P, Paris S, Antonny B, Robineau S, Beraud-Dufour S, Jackson CL, Chabre M: **A human exchange factor for ARF contains Sec7- and pleckstrin-homology domains.** *Nature* 1996, **384**(6608):481–484.
18. Jackson CL, Casanova JE: **Turning on ARF: the Sec7 family of guanine-nucleotide-exchange factors.** *Trends Cell Biol* 2000, **10**(2):60–67.
19. Betz SF, Schnuchel A, Wang H, Olejniczak ET, Meadows RP, Lipsky BP, Harris EA, Staunton DE, Fesik SW: **Solution structure of the cytohesin-1 (B2-1) Sec7 domain and its interaction with the GTPase ADP ribosylation factor 1.** *Proc Natl Acad Sci U S A* 1998, **95**(14):7909–7914.
20. Cherfils J, Menetrey J, Mathieu M, Le Bras G, Robineau S, Beraud-Dufour S, Antonny B, Chardin P: **Structure of the Sec7 domain of the Arf exchange factor ARNO.** *Nature* 1998, **392**(6671):101–105.
21. Franco M, Peters PJ, Boretto J, van Donselaar E, Neri A, D'Souza-Schorey C, Chavrier P: **EFA6, a sec7 domain-containing exchange factor for ARF6, coordinates membrane recycling and actin cytoskeleton organization.** *EMBO J* 1999, **18**(6):1480–1491.
22. Frank S, Upender S, Hansen SH, Casanova JE: **ARNO is a guanine nucleotide exchange factor for ADP-ribosylation factor 6.** *J Biol Chem* 1998, **273**(1):23–27.
23. Mossessova E, Gulbis JM, Goldberg J: **Structure of the guanine nucleotide exchange factor Sec7 domain of human arno and analysis of the interaction with ARF GTPase.** *Cell* 1998, **92**(3):415–423.
24. Shevell DE, Leu WM, Gillmor CS, Xia G, Feldmann KA, Chua NH: **EMB30 is essential for normal cell division, cell expansion, and cell adhesion in Arabidopsis and encodes a protein that has similarity to Sec7.** *Cell* 1994, **77**(7):1051–1062.
25. Thompson JD, Gibson TJ, Higgins DG: **Multiple sequence alignment using ClustalW and ClustalX.** *Curr Protoc Bioinformatics* 2002, **2**:2–3.
26. Shi J, Blundell TL, Mizuguchi K: **FUGUE: sequence-structure homology recognition using environment-specific substitution tables and structure-dependent gap penalties.** *J Mol Biol* 2001, **310**(1):243–257.
27. Li H, Wei S, Cheng K, Gounko NV, Ericksen RE, Xu A, Hong W, Han W: **BIG3 inhibits insulin granule biogenesis and insulin secretion.** *EMBO Rep* 2014, **15**(6):714–722.
28. Hirose S, Shimizu K, Kanai S, Kuroda Y, Noguchi T: **POODLE-L: a two-level SVM prediction system for reliably predicting long disordered regions.** *Bioinformatics* 2007, **23**(16):2046–2053.
29. Shimizu K, Muraoka Y, Hirose S, Tomii K, Noguchi T: **Predicting mostly disordered proteins by using structure-unknown protein data.** *BMC Bioinformatics* 2007, **8**:78.
30. Ishida T, Kinoshita K: **PrDOS: prediction of disordered protein regions from amino acid sequence.** *Nucleic Acids Res* 2007, **35**(Web Server issue):W460–W464.

31. Mizuguchi K, Deane CM, Blundell TL, Johnson MS, Overington JP: **JOY: protein sequence-structure representation and analysis.** *Bioinformatics* 1998, **14**(7):617–623.
32. Murakami Y, Mizuguchi K: **Applying the Naive Bayes classifier with kernel density estimation to the prediction of protein-protein interaction sites.** *Bioinformatics* 2010, **26**(15):1841–1848.
33. Zidovetzki R, Rost B, Armstrong DL, Pecht I: **Transmembrane domains in the functions of Fc receptors.** *Biophys Chem* 2003, **100**(1–3):555–575.
34. Ahmad S, Mizuguchi K: **Partner-aware prediction of interacting residues in protein-protein complexes from sequence data.** *PLoS One* 2011, **6**(12): e29104.
35. Stark C, Breitkreutz BJ, Reguly T, Boucher L, Breitkreutz A, Tyers M: **BioGRID: a general repository for interaction datasets.** *Nucleic Acids Res* 2006, **34**(Database issue):D535–D539.
36. Yamasaki C, Murakami K, Fujii Y, Sato Y, Harada E, Takeda J, Taniya T, Sakate R, Kikugawa S, Shimada M, Tanino M, Koyanagi KO, Barrero RA, Gough C, Chun HW, Habara T, Hanaoka H, Hayakawa Y, Hilton PB, Kaneko Y, Kanno M, Kawahara Y, Kawamura T, Matsuya A, Nagata N, Nishikata K, Noda AO, Nurimoto S, Saichi N, Sakai H, *et al*: **The H-Invitational Database (H-InvDB), a comprehensive annotation resource for human genes and transcripts.** *Nucleic Acids Res* 2008, **36**(Database issue):D793–D799.
37. Emerson V, Holtkotte D, Pfeiffer T, Wang IH, Schnolzer M, Kempf T, Bosch V: **Identification of the cellular prohibitin 1/prohibitin 2 heterodimer as an interaction partner of the C-terminal cytoplasmic domain of the HIV-1 glycoprotein.** *J Virol* 2010, **84**(3):1355–1365.
38. Hwang C, Giri VN, Wilkinson JC, Wright CW, Wilkinson AS, Cooney KA, Duckett CS: **EZH2 regulates the transcription of estrogen-responsive genes through association with REA, an estrogen receptor corepressor.** *Breast Cancer Res Treat* 2008, **107**(2):235–242.
39. Kasashima K, Ohta E, Kagawa Y, Endo H: **Mitochondrial functions and estrogen receptor-dependent nuclear translocation of pleiotropic human prohibitin 2.** *J Biol Chem* 2006, **281**(47):36401–36410.
40. Ross JA, Nagy ZS, Kirken RA: **The PHB1/2 phosphocomplex is required for mitochondrial homeostasis and survival of human T cells.** *J Biol Chem* 2008, **283**(8):4699–4713.
41. Clamp M, Cuff J, Searle SM, Barton GJ: **The Jalview Java alignment editor.** *Bioinformatics* 2004, **20**(3):426–427.
42. McGuffin LJ, Bryson K, Jones DT: **The PSIPRED protein structure prediction server.** *Bioinformatics* 2000, **16**(4):404–405.
43. McDonnell AV, Jiang T, Keating AE, Berger B: **Paircoil2: improved prediction of coiled coils from sequence.** *Bioinformatics* 2006, **22**(3):356–358.
44. Lupas A, Van Dyke M, Stock J: **Predicting coiled coils from protein sequences.** *Science* 1991, **252**(5009):1162–1164.
45. Andrade MA, Ponting CP, Gibson TJ, Bork P: **Homology-based method for identification of protein repeats using statistical significance estimates.** *J Mol Biol* 2000, **298**(3):521–537.
46. Soding J, Remmert M, Biegert A: **HHrep: de novo protein repeat detection and the origin of TIM barrels.** *Nucleic Acids Res* 2006, **34**(Web Server issue):W137–W142.
47. George RA, Heringa J: **The REPRO server: finding protein internal sequence repeats through the Web.** *Trends Biochem Sci* 2000, **25**(10):515–517.
48. Soding J: **Protein homology detection by HMM-HMM comparison.** *Bioinformatics* 2005, **21**(7):951–960.

doi:10.1186/1756-0500-7-435
Cite this article as: Chen *et al.*: Brefeldin a-inhibited guanine nucleotide-exchange protein 3 (BIG3) is predicted to interact with its partner through an ARM-type α-helical structure. *BMC Research Notes* 2014 **7**:435.

NF-κB signaling mediates acquired resistance after PARP inhibition

Yuko Nakagawa[1,2,*], Anna S. Sedukhina[1,*], Naoki Okamoto[2], Satoi Nagasawa[1,3], Nao Suzuki[2], Tomohiko Ohta[1], Hiroyoshi Hattori[4], Marta Roche-Molina[5], Ana J. Narváez[6], Anand D. Jeyasekharan[7], Juan A. Bernal[5], Ko Sato[1]

[1]Department of Translational Oncology, St. Marianna University Graduate School of Medicine, Kawasaki 216-8511, Japan

[2]Department of Obstetrics and Gynecology, St. Marianna University Graduate School of Medicine, Kawasaki 216-8511, Japan

[3]Division of Breast and Endocrine Surgery, Department of Surgery, St. Marianna University Graduate School of Medicine, Kawasaki 216-8511, Japan

[4]Laboratory of Advanced Therapy, Department of Hematology and Oncology Research, Clinical Research Center, National Hospital Organization Nagoya Medical Center, Nagoya 460-0001, Japan

[5]Department of Cardiovascular Development and Repair, Centro Nacional de Investigaciones Cardiovasculares (CNIC), Madrid 28029, Spain

[6]MRC Cancer Unit at the University of Cambridge, Hutchison Research Centre, CB2 0XZ, UK

[7]Cancer Science Institute of Singapore, National University of Singapore, Centre for Translational Medicine, 117599, Singapore

[*]These authors have contributed equally to this work

Correspondence to:
Ko Sato, **e-mail:** kosato@marianna-u.ac.jp

Received: August 12, 2014 ***Accepted:*** December 07, 2014 ***Published:*** January 13, 2015

ABSTRACT

PARP inhibitors are a class of promising anti-cancer drugs, with proven activity in *BRCA* mutant cancers. However, as with other targeted agents, treatment with PARP inhibitors generates acquired resistance within these tumors. The mechanism of this acquired resistance is poorly understood. We established cell lines that are resistant to PARP inhibitor by continuous treatment with the drug, and then used RNA sequencing to compare gene expression. Pathway analysis on the RNA sequencing data indicates that NF-κB signaling is preferentially up-regulated in PARP inhibitor-resistant cells, and that knockdown of core components in NF-κB signaling reverses the sensitivity to PARP inhibitor in resistant cells. Of therapeutic relevance, we show that PARP inhibitor-resistant cells are sensitive to an NF-κB inhibitor in comparison to their parental controls. Malignancies with up-regulation of NF-κB are sensitive to bortezomib, a proteasome inhibitor that is currently used in the clinic. We also show that treatment with bortezomib results in cell death in the PARP inhibitor-resistant cells, but not in parental cells. Therefore we propose that up-regulation of NF-κB signaling is a key mechanism underlying acquired resistance to PARP inhibition, and that NF-κB inhibition, or bortezomib are potentially effective anti-cancer agents after the acquisition of resistance to PARP inhibitors.

INTRODUCTION

Patients with the hereditary breast and ovarian cancer syndrome (HBOCS) commonly have mutations in the key genome stability proteins, *BRCA1* and *BRCA2*. Research over the last decade has yielded a promising therapeutic strategy for *BRCA* mutant cancers, through the observation that cells mutant for the *BRCA* genes are exquisitely sensitive to inhibition of the nuclear enzyme poly-adenosine ribose polymerase (PARP), through a synthetic lethal mechanism. These observations have been borne out in early phase clinical trials, with promising activity of PARP inhibitors both in breast and ovarian cancers [1–3]. In ovarian cancer, a recent phase II study has demonstrated a benefit of maintenance PARP inhibition in the management of metastatic ovarian cancers [4]. As with all maintenance therapeutic strategies, the development of resistance to prolonged single agent therapy is inevitable,

thus necessitating the study of mechanisms of resistance and the development of therapeutic strategies to overcome them. Currently explored mechanisms for acquired resistance to PARP inhibition include 1. Reversion of the mutation of *BRCA* gene [5, 6], 2. Disruption of 53BP1 [7], 3. Up-regulation of p-glycoprotein efflux pump [8] and 4. Phosphorylation of ribosomal protein S6 [9]. However, there are no reports to date of a comprehensive screening approach to investigate the mechanism of resistance to PARP inhibition, especially in the context of ovarian cancer where maintenance PARP inhibitor therapy is of clinical benefit.

In this paper, we describe our studies comparing PARP inhibitor resistant and sensitive clones, and show an up-regulation of Nuclear Factor- κB (NF-κB) pathways in the resistant clones. NF-κB is a complex of transcription factors that consisting of p65 (RelA) and p50 (NFκB1) or RelB and p52 (NFκB2), that are known to function in the development of acquired resistance to several other targeted agents [10]. NF-κB signaling has two major pathways, one is the canonical pathway that mainly modulates cell proliferation, inflammation or anti-apoptosis, and the other one is the non-canonical pathway that mainly controls lymphogenesis and B cell maturation [11]. In the canonical pathway, p65/p50 NF-κB complex are localized in cytoplasm with IκB. Stimuli such as infection, cytokines, apoptosis-inducers activate NF-κB in canonical pathway. Binding those stimuli to their receptors including tumor necrosis factor receptor (TNFR) or interleukin 1 (IL-1) receptor (IL-1R) activates the IκB kinase (IKK) complex. The activated IκB kinase complex phosphorylates IκB and the phosphorylated IκB is degraded by β-TRCP-dependent ubiquitination. This results in nuclear translocation of p65/p50 heterodimer and activates transcription of NF-κB target genes [10]. In non-canonical pathway, p100, a precursor of p52, is a central player. p100 binds to RelB and stays in cytoplasm in non-activated state. Once activated via a binding of ligands including BAFF (B cell activating factor, a family member of TNF) to their receptors, p100 is processed to p52 and RelB/p52 heterodimer is translocated into nucleus to activate transcription of NF-κB target genes [12].

NF-κB inhibition rescues the sensitivity to anti-cancer drug in chemoresistant cancer cells, through TNFα mediated apoptosis, and indeed increases tumor regression [13]. Thus, NF-κB plays an important role in chemoresistance, and our paper describes a new role for this pathway in mediating resistance to PARP inhibition as well.

RESULTS

Establishment of PARP inhibitor resistant clone

We used UWB1.289 ovarian cancer cells and HCC1937 breast cancer cells as parental cell lines to generate PARP inhibitor-resistant lines. Both the cell lines harbor homozygous mutation of *BRCA1*. PARP inhibitor-resistant clones (R10 and R100 in UWB1.289 and R500 in HCC1937) were developed independently by repeated exposure to different doses of PARP inhibitor (Olaparib AZD2281, KU-0059436) (10nM, 100nM and 500nM, respectively). To generate PARP inhibitor-resistant lines, we have used olaparib (AstraZeneca), a PARP inhibitor that is most advanced in clinical development, and currently in phase III testing [1–4]. For checking resistance to PARP inhibition, we used 2 distinct compounds- olaparib and rucaparib (AG014699; Clovis). While olaparib showed promising results in phase II studies in patients with breast and ovarian cancers having *BRCA* mutations [4], rucaparib was initially established as a radiosensitizer and to potentiate the effect of temozolamide. Phase II/ III trials are currently underway for both these agents with preliminary results of activity in BRCA mutant cancers [14]. Both the olaparib and rucaparib are bona fide PARP inhibitors and inhibit both PARP1 and PARP2 [14]. Both of the compounds have similar potency in inhibiting PARP catalytic activity [14–16]. The PARP inhibitor-resistant lines show decreased sensitivity to both olaparib and rucaparib, both in UWB1.289 setting- R10/R100 (Figure 1A and 1B) and in the HCC1937 setting- R500 (Figure 1C and 1D).

Validation of reported mechanisms for PARP inhibitor-resistance

Several mechanisms for acquired resistance to PARP inhibition have been already proposed [5–9]. Therefore, prior to exploring a new mechanism with a comprehensive screening in PARP inhibitor-resistant cells, we have tested whether any of these reported mechanisms were responsible for PARP inhibitor-resistance in our PARP inhibitor-resistant lines. One reported mechanism for acquired resistance to PARP inhibition is a reversion of *BRCA1* gene mutation [6]. Therefore we checked the sequence of *BRCA1* gene. The mutations of *BRCA1* genes are conserved in all the resistant lines (Figure 2A and 2B). Another reported mechanism is disruption of 53BP1 function [7]. Treatment with DNA damaging agents such as camptothecin, a topoisomerase I inhibitor, induces 53BP1 foci formation when 53BP1 is functional [17]. All the parental and PARP inhibitor-resistant UWB1.289 or HCC1937 cells display similar level of induction of 53BP1 foci formation with elevation of γH2AX signal, a surrogate marker of DNA double strand breaks, in response to camptothecin (Figure 2C–2F and Supplementary Figure 1) [18]. These results suggest that 53BP1 is functional in the PARP inhibitor-resistant lines. Other reports suggest that up-regulation of p-glycoprotein efflux pump *Abcb1a* (as defined by mRNA expression), is a possible mechanism for PARP inhibitor-resistance [8]. mRNA expression of *Abcb1a* in parental and PARP inhibitor-resistant UWB1.289 or HCC1937 cells was investigated and the expression of

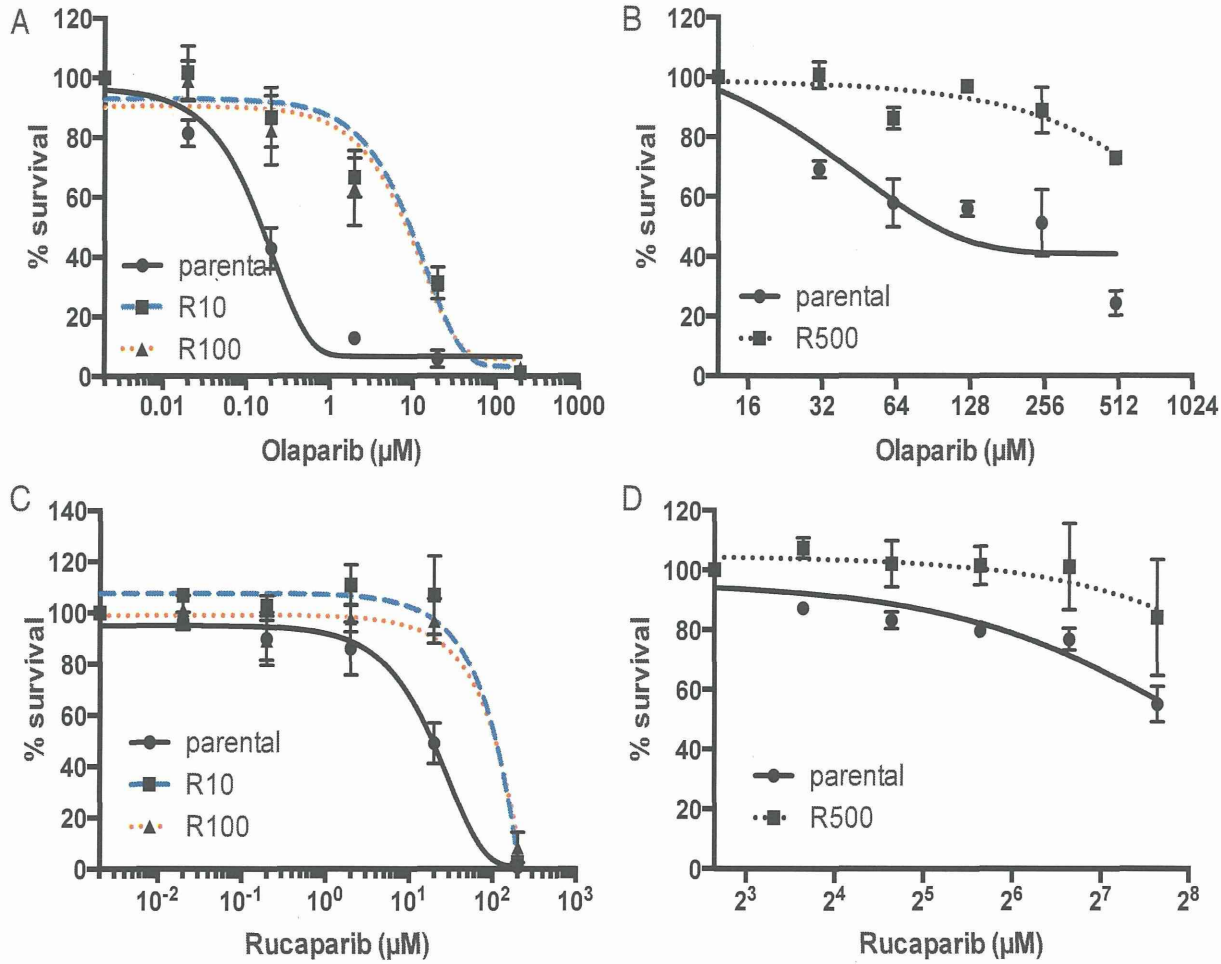

Figure 1: Sensitivity to PARP inhibitor in UWB1.289 cells. Line chart shows the sensitivity to olaparib **(A)** and **(B)** or rucaparib **(C)** and **(D)** in parental or PARP inhibitor-resistant UWB1.289 cells **(A)** and **(C)** and in HCC1937 cells **(B)** and **(D)**. Error bar shows standard deviation of three independent experiments.

the *Abcb1a* is not altered through the lines (Figure 2G and 2H). An additional mechanism reported for resistance to PARP inhibition is excess phosphorylation of ribosomal protein S6 [9]. However, this is also not applicable in our PARP inhibitor-resistant clones (Figure 2I). Therefore we explored a new mechanism for resistance to PARP inhibition using our clones with acquired resistance, using a comprehensive screening approach.

RNA sequencing to compare PARP inhibitor-resistant and sensitive clones of the ovarian cell line UWB1.289

We performed whole transcriptome RNA sequencing of cDNA libraries derived from parental UWB1.289, and the PARP inhibitor-resistant clones R10 and R100. We obtained reads to the order of ~13 million (parental) and ~14 million (R10 and R100) (Supplementary Figure 2). Among these reads of parental, R10 and R100, 81 to 85% of them were mapped to human genome GRCh37. Using Rsem and EdgeR analysis, we identified differentially expressed genes (DEGs) among the parental, R10 and R100 (parental vs R10 and parental vs R100) [19, 20].

Pathway analysis for acquired resistance to PARP inhibition

Next we used Ingenuity Pathway Analysis (IPA) to identify the DEGs in the common pathways. IPA is a web-based software to analyze RNA sequencing data to understand relation to large biological systems [21]. In order to obtain meaningful output, we identified DEGs by log ratio ≥ 2 and p-value $\leq$ 5.00E-02. In this setting, we identified 118 DEGs (parental vs R10) and 85 DEGs (parental vs R100). IPA with DEGs for parental vs R10 or parental vs R100 shows significant enrichment of genes in category of "Cancer" among the other categories (Supplementary Table 1). To identify the exact pathway

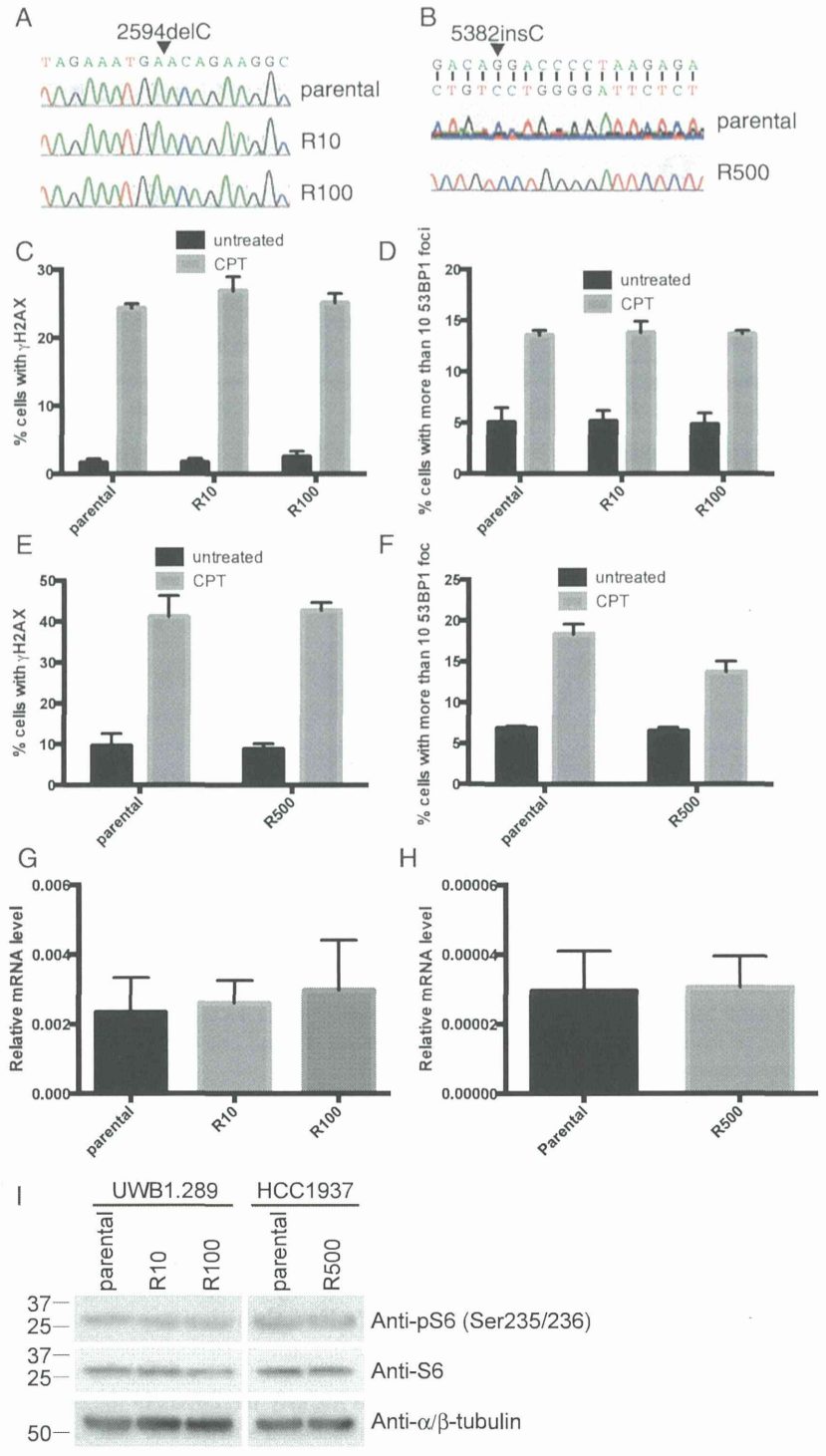

Figure 2: Known mechanisms for PARP inhibitor-resistance are not applicable. Direct sequencing of *BRCA1* gene in UWB1.289 **(A)** and HCC1937 **(B)** are shown. Cells were treated with CPT (camptothecin: 3μM) for 3 hours and stained with antibodies against γH2AX and 53BP1. Untreated cells were also stained as control. Histogram shows ratio of γH2AX positive cells in UWB1.289 **(C)** and in HCC1937 **(E)** and ratio of cells with more than 10 53BP1 foci in UWB1.289 **(D)** and in HCC1937 **(F)**. Error bar shows standard deviation of three independent experiments. Histogram shows mRNA expression of *Abcb1a* in parental and PARP inhibitor-resistant UWB1.289 **(G)** or HCC1937 **(H)**. Error bar shows standard deviation of three independent experiments. Cell lysates from parental or PARP inhibitor-resistant UWB1.289 or HCC1937 cells were subjected for western blotting with indicated antibodies **(I)**.